Three-Dimensional Base Isolation Using Vertical Negative Stiffness Devices

THREE-DIMENSIONAL BASE ISOLATION USING VERTICAL NEGATIVE STIFFNESS DEVICES

G.P. Cimellaro[1], M. Domaneschi [2], G. Warn[3]

ABSTRACT

A 3-D base isolation system to control both the horizontal and vertical components of ground motion is presented in this paper. The system is adopting a negative stiffness device that can be considered as an adaptive passive protection system, which can apparently change the stiffness of the structure. This work is focused on studying through numerical simulations the mitigation performance of the negative stiffness device against strong earthquakes in the vertical direction. The base isolation arrangement consists of elastomeric bearings acting both in the horizontal and vertical direction and negative stiffness devices acting only in the vertical direction. So, a three-dimensional base isolation is achieved, where it is assumed that the negative stiffness devices affect the vertical stiffness of the system only. Numerical analyses show that the presence of negative stiffness devices reduces the vertical acceleration in the structure. Nevertheless, accordingly with the passive control theory, the relative displacements increase. Therefore, it seems advisable a supplemental damping to mitigate this effect. Thanks to the presence of rubber isolators, it is possible to employ their inherent damping without introducing specific dampers in the vertical direction.

KEYWORDS**:** negative stiffness, vertical, three-dimensional base isolation, passive control, near field ground motion

INTRODUCTION

Typically, while a conventional seismic isolation system reduces the horizontal component of an earthquake, the vertical component is entirely transmitted in the structure. Therefore, the interest

[1] Associate Professor, Department of Structural, Building And Geotechnical Engineering (DISEG), Politecnico di Torino, 10129 Turin, Italy (gianpaolo.cimellaro@polito.it)
[2] Assistant Professor, Department of Structural, Building And Geotechnical Engineering (DISEG), Politecnico di Torino, 10129 Turin, Italy (marco.domaneschi@polito.it)
[3] Associate Professor, Department of Civil and Environmental Engineering, Penn State University | 226B Sackett Building - University Park, PA 16802 USA (e-mail: gwarn@engr.psu.edu)

toward three-dimensional (3-D) isolation systems is increasing. In literature can be found some examples of application of 3-D base isolations systems that consists in modifying the design parameters of laminated rubber bearings [ID Aiken 1989; Kelly 1988; Okamura et al. 2011].

The GERB system [JM Kelly 1990] has been introduced in 1990 and consists of helical steel springs that are flexible horizontally and vertically. The spring is essentially undamped so it needs to be used in conjunction with supplemental dampers. The system has been applied in two buildings in California. Limitations can be identified in the coupling between the horizontal and the vertical motion due to geometric nonlinearities.

Suhara [Suhara 2003] developed a 3-D seismic isolation device that uses a laminated rubber bearing for the horizontal direction and a rolling seal type air spring in the vertical direction. The issue of concern for this device are the pitching and rolling effects, so it needs to be used in combination with a rocking suppression system.

3-D seismic isolation systems for the protection of nuclear power plants can be found in the literature. Different solutions are proposed, as the 3-D base isolation of the entire building or the vertical isolation of the main structural components associated to horizontal building base isolation [Inoue 2004; Morishita 2004].

The protection of structures through constant load spring devices against near-field earthquakes, characterized by a vertical component of the same intensity as the horizontal ones, is investigated in [Asai 2008].

Hybrid control solutions have been also studied for developing a 3-D vibration isolation system assembling mechanical and electromagnetic units [Hoque 2011].

A recent MCEER report compares different alternatives to seismically isolate electrical transformers. In particular, the performance of non-isolated, horizontally isolated and 3-D isolated

solutions are analyzed considering triple friction pendulum (FP) devices in horizontal direction and viscous dampers in the vertical one [Kitayama 2016].

This paper considers as an alternative idea to insert a negative stiffness device (NSD) in the vertical direction only, within a conventional base isolation system.

The concept of negative stiffness has been first introduced in the pioneering publication of Molyneaux [Molyneaux 1957; Molyneaux 1957] in several proposals for vibration isolation systems. Later an effective passive negative-stiffness isolator that uses mechanical concept only in low-frequency vibration isolation has been proposed by Platus [Platus 1991; Platus 2007]. The isolation of the vertical-motion is provided by a stiff spring that supports a weight load, combined with a negative-stiffness mechanism. The limitation with this device is that it requires preload forces of the order of the supported weight. Therefore, it is usually employed for special equipment of lightweight real applications.

So far, the application of NSDs has been limited to vibration isolation of small, highly sensitive equipment and of seats in automobiles [Lee et al. 2007], because large forces (typically the same order of the weight of the building) are required to develop negative stiffness.

Some examples of applications of a pseudo-negative stiffness system for civil engineering structures have been also developed. “Negative” hysteresis loops are firstly achieved using a hydraulic device that is fully active or semi-active [Iemura and Pradono 2003]. Then, Iemura et al. [Iemura et al. 2006] proposed a variable damper with a combination of friction loops with pseudo negative stiffness (“negative” hysteresis loops), to reduce the acceleration of the structure along with displacements. In [H Iemura 2008] a structure is placed on top of convex pendulum bearings, exactly the opposite with respect to friction pendulum bearings which use a concave surface. So the negative stiffness is generated from the structure’s vertical loads applied on the

convex surface, while the elastomeric bearings are placed in parallel to provide positive stiffness. However, the reliance of variable damper on the external power and feedback signal to generate the negative hysteresis loops limits its applications. A negative stiffness is regarded as one of the promising control strategies in view of absolute response reduction except that such a control requires, in general, active or semi-active devices [Soong and Cimellaro 2009].

The concept of NSD presents some similarities with the retrofit system based on weakening and damping (WeD) the structure [Cimellaro et al. 2009; Reinhorn et al. 2009; Viti et al. 2006], however even though weakening and damping of structures is capable of reducing both the accelerations and the interstory drifts, it generates damage and permanent deformations.

Nagarajaiah et al. [Nagarajaiah et al. 2010] have proposed the concept of "apparent weakening" where the NSD is employed to simulate the yielding of the global system (weakening) without changing the real stiffness of the structure. Therefore, it allows to move the system away from the resonance condition. Practically, a pseudo yielding is created that is below the real yielding of the structure. The NSD is designed not to transfer forces to the structure until the displacement is greater than the gap displacement (displacement when occurs the pseudo-yielding). Nevertheless, the proposed concept at this stage results impractical for large structures.

In order to attain the negative stiffness more economically, a new structural control device that realizes a negative stiffness in a passive manner has been firstly proposed by Sarlis et al. [Sarlis et al. 2013] and tested on a shaking table at the University at Buffalo [Pasala et al. 2013; Pasala et al. 2014].

Apparent weakening behavior and the negative stiffness device performance have been more recently deepened analytically and experimentally using shaking table tests [Attary et al. 2015; Pasala et al. 2015; Sarlis et al. 2016].

However, to the authors' knowledge, limited studies for the application in civil engineering of the concept of NSD to reduce the vertical accelerations in base isolated buildings can be found in literature, trying to reach what can be called three-dimensional base isolation. E.g. a theoretical study for 3-D base isolation using a negative stiffness mechanism is investigated for possible applications [Mochida 2015]. More negative stiffness and quasi-zero stiffness designs also exist [P. Alabuzhev 1989].

Certainly, the negligible vertical performance in earthquake effect mitigation of conventional base isolation systems is well known. It spans from rubber bearing to friction pendulum systems and rolling systems. Considering the most common class of elastomeric bearings, their inherent strong vertical stiffness does not allow to isolate the seismic response excited by a vertical ground motion. Some innovative attempts and solutions for overcoming the isolation limits in the vertical direction have been proposed: 3-D steel springs arrangements and fiber reinforced elastomeric bearings can be mentioned [Harvey 2016; Kelly and Van Engelen 2016; Li et al. 2013].

This paper presents an innovative 3-D base isolation system that adopts a NSD for vibration mitigation in the vertical direction, combined with elastomeric devices acting in the horizontal plane. The main assumption is that the NSD is self-contained and therefore when installed it affects only the vertical stiffness of the system while leaving the horizontal stiffness equal to the stiffness of the isolators. In other words, the NSD does not participate in transferring the horizontal loads [AA Sarlis 2011; Perotti et al. 2013].

Applications of NSDs in the vertical direction for vibration mitigation of heavy structures are extremely difficult or impossible to arrange for the enormous reaction forces required. On the contrary, light highly sensitive equipment or sculptures and artistic masterworks could be effectively protected by the proposed 3-D base isolation system proposed.

The numerical results of a base isolated single-degree-of-freedom (SDOF) system with a NSD installed at the isolator level in parallel with the rubber bearings are reported. Three different systems: (i) fixed base, (ii) isolated and (iii) isolated with NSD are compared for a suite of selected ground motions. The numerical results show that by adding the NSD in the vertical direction it is possible to reduce the vertical seismic forces in the structure.

CHARACTERISTICS OF NEGATIVE STIFFNESS DEVICES

The NSD has been designed during a joint project between the University of Buffalo, Rice University and Taylor Devices Inc. and it has been tested extensively in the last years on the shaking table of the University at Buffalo. When applied in the horizontal direction, as for the original implementation, it exhibits true negative stiffness, and it is able to generate a force that pushes the isolated structure in the same direction of the seismic induced relative horizontal displacement between the base and the ground (not in the opposite as in the case of positive stiffness). The true negative stiffness for structural applications is a concept that has been first introduced by Nagarajaiah et al. [S Nagarajaiah 2010] and can be accomplished without any external power supply, as in the case of pseudo-negative stiffness of active and semi-active devices. The NSD can be classified as a passive seismic protection system but it belongs to a more sophisticated typology, the adaptive one. It means that it can change its characteristics when it deforms. Furthermore, even it is a self-contained and inherently unstable device, the NSD can show a stable behavior when implemented in a structure; in other words, it is the structure that stabilizes the device.

The negative stiffness is generated through a pre-compressed spring at the center between two chevron braces, designed to contain the high compressive force of the spring. When the NSD deforms, the spring rotates and extends giving a force that assists the structure.

The NSD simulates an apparent weakening without changing the real stiffness of the structure, in order to move the system appropriately far from the resonance condition. In other words, a pseudo yielding is created, that is below the real yielding of the structure.

The NSD is designed to transfer almost zero forces to the structure until the displacement is greater than the gap displacement (displacement at which occurs the pseudo yield). To generate such behavior a so called Gap Spring Assembly (GSA) is implemented. It consists in a couple of mechanical springs, generating bilinear elastic positive stiffness. When the displacement is smaller than the gap, the GSA is able to cancel out the negative stiffness. On the contrary, when the displacement overcome the gap threshold, the stiffness of the GSA is close to zero, hence the negative stiffness of the device is transferred to the structure.

The NSD has been originally used in parallel with passive dampers. Actually, the apparent reduction of stiffness produces an increment of displacement that has to be controlled. Therefore, a small amount of damping is needed.

Details on NSD can be found in Sarlis et al.[Sarlis et al. 2013], where the force-displacement law for the NSD without GSA, the GSA and the combination of them is presented. Figure 1a depicts the force-displacement laws for the main structure (linear elastic), a linear passive damper and the NSD with GSA. Figure 1b shows the bilinear behavior coming from the structure in parallel with NSD and GSA without damper. The structure + NSD assembly stiffness reduces to $K_a=K_s-K_{NSD}$ beyond the displacement y_1. If F_2 and y_2 are the maximum force and displacement for the linear system, F_3 and y_3 are the same variable, but related to the assembly. The maximum displacement

y_3 results increased with respect to the linear stiffness y_2 ($y_3 > y_2$). So, the introduction of a damper in parallel with the NSD and the spring allows an improved response in terms of displacement y'_3 (Figure 1c).

A further positive characteristic of the composite NSD, GSA and the isolated structural system is that it is able to re-center. Therefore, residual deformations at the base isolation level is restored, unless the main structure itself developed plastic deformations due to yielding.

In this work, for the sake of simplicity, the *NSD function* is adopted with a bilinear model in the vertical direction only. In the horizontal plane, uncoupled isolation function coming from rubber bearings is implemented. As the rubber isolators have already an intrinsic damping capacity, this latter can be useful for limiting the relative vertical displacements.

DESCRIPTION OF THE MODEL ADOPTED

The effectiveness of the NSD for the mitigation of the vertical vibrations has been assessed using a standard structure. It consists in a 2-D frame, one story and one bay with general dimensions and characteristics. The case study is not related to a specific application, but it serves as a useful benchmark for assessing the effectiveness of the NSD in the vertical direction. It consists in two columns and a rigid horizontal beam. The span measures 9.15 m and the height is 3.96 m. The mass distributed on the beam is 160000 kg. The frame has a total horizontal stiffness of 77000 kN/m, so the corresponding period of vibration is T_H = 0,28 s. The total vertical stiffness of the frame is 5.7×10^6 kN/m, hence the vertical period is T_V = 0,033 s. The damping ratio for this structure is assumed ξ=5% and it has been included in the equation of motion using the Rayleigh damping matrix.

The performance of three structural arrangements are compared: (i) a fixed base structure, (ii) a rubber bearings horizontally isolated structure and (iii) a rubber bearings horizontally isolated structure with decoupled NSD in the vertical direction. The fixed base structure (i) and the isolated superstructure (ii and iii) correspond to the frame and the parameters described at the beginning of this section. However, the three studied typologies are described in detail in what follows:

1) Fixed base structure:

The horizontal beam is assumed rigid, the columns deformable and fixed at the base, therefore the frame has three degrees of freedom: the horizontal displacement, the vertical displacement and the rotation angle in the vertical plane (the displacements are referred to the centroid of the beam). The stiffness matrix results:

$$\begin{bmatrix} T \\ N \\ M \end{bmatrix} = \begin{bmatrix} 2\cdot\frac{12EI}{h^3} & 0 & 2\cdot\frac{6EI}{h^2} \\ 0 & 2\cdot\frac{EA}{h} & 0 \\ 2\cdot\frac{6EI}{h^2} & 0 & 2\cdot\left(\frac{4EI}{h}+\frac{EA}{h}\cdot\frac{L^2}{4}\right) \end{bmatrix} \begin{bmatrix} x \\ y \\ \theta \end{bmatrix} \quad (1)$$

where T, N, M are the internal forces in the columns: respectively shear force, axial force, bending moment. E is the Young modulus, h the total length, A and I the cross section area and inertia, L the distance between the columns (Figure 2a). The term K_{11} is 77000kN/m, while K_{22} is 5.7×10^6 kN/m.

The governing dynamic equations are presented in Equation (2), where the damping matrix is omitted. The mass matrix is diagonal and the term corresponding to the rotation degree of freedom is the moment of inertia of the beam. The right side of the equation reports the forces coming from the ground motion. Obviously, the rotational part is negligible.

$$\begin{bmatrix} m & 0 & 0 \\ 0 & m & 0 \\ 0 & 0 & \frac{mL^2}{12} \end{bmatrix} \begin{bmatrix} \ddot{x} \\ \ddot{y} \\ \ddot{\theta} \end{bmatrix} + \begin{bmatrix} 2\cdot\frac{12EI}{h^3} & 0 & 2\cdot\frac{6EI}{h^2} \\ 0 & 2\cdot\frac{EA}{h} & 0 \\ 2\cdot\frac{6EI}{h^2} & 0 & 2\cdot\left(\frac{4EI}{h}+\frac{EA}{h}\cdot\frac{L^2}{4}\right) \end{bmatrix} \begin{bmatrix} x \\ y \\ \theta \end{bmatrix} = -\begin{bmatrix} m & 0 & 0 \\ 0 & m & 0 \\ 0 & 0 & \frac{mL^2}{12} \end{bmatrix} \begin{bmatrix} \ddot{x}_g \\ \ddot{y}_g \\ 0 \end{bmatrix} \quad (2)$$

With reference to Equation (2), m is the mass, x, y, θ the Lagrangian coordinates, $\ddot{x}_g$, $\ddot{y}_g$ the ground motion acceleration components in the horizontal and the vertical direction respectively. Over-dot represents the derivative with respect to time. It is evident how the vertical motion is uncoupled from the other two.

2) Isolated structure

(

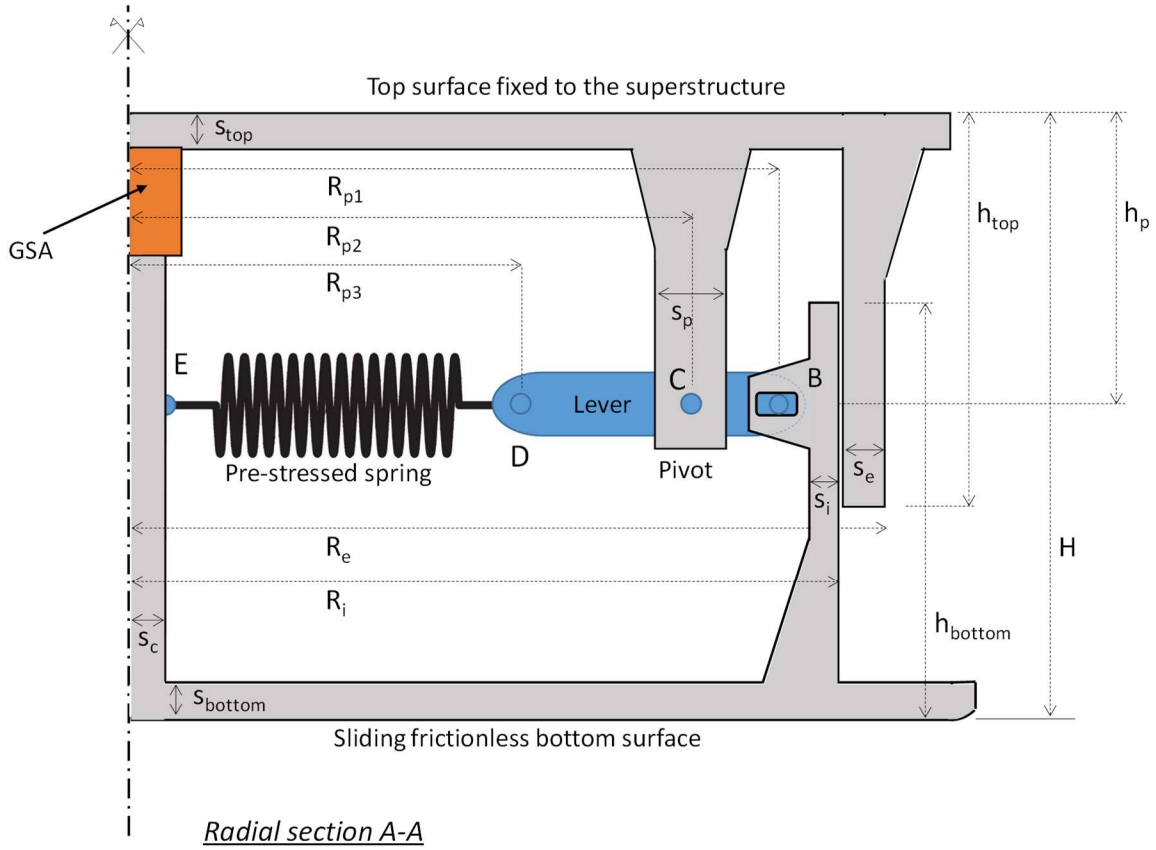

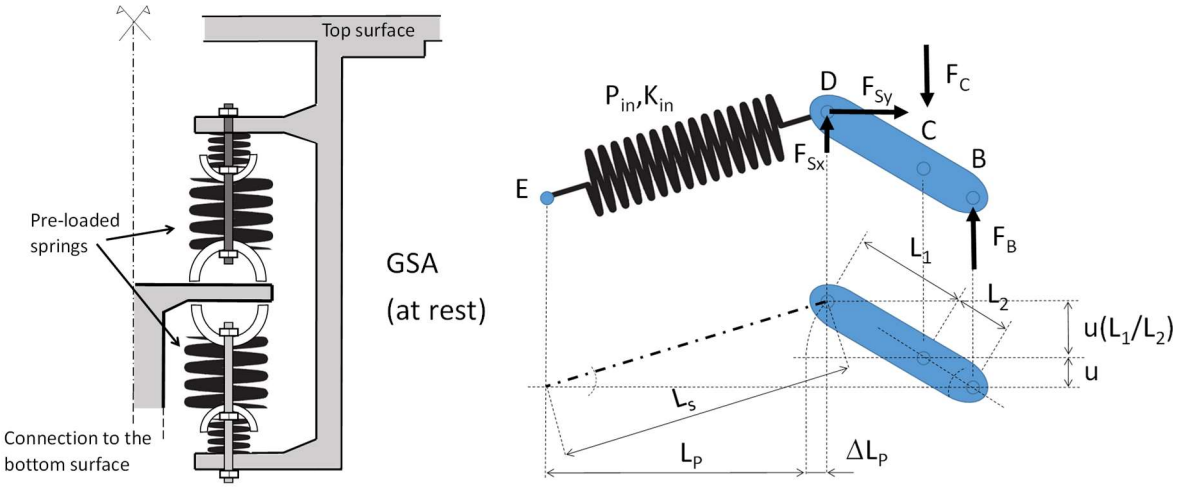

Figure 2*a without the NSD device):*

For this configuration, another floor at the base isolation level is added and two rubber isolators support it. The floor is assumed rigid and has the same mass *m* of the floor over the deformable columns. The new degrees of freedoms are the horizontal and vertical displacements of the mass centroid (x_1, y_1) at the isolation level. The rotation at this level is not considered: in other words, the rocking motion is disregarded at the isolation level. At the end, five degrees of freedom are considered in the structure.

Each isolator has a fixed damping ratio of 15% and their behavior is assumed linear elastic. This value is typical for high damping rubber bearings, or lead rubber bearings, at larger cycles of hysteresis [Abe et al. 2004; Perotti et al. 2013], where the benefits coming from the base isolation system, in terms of dissipation and system decoupling from the ground motion, are more evident. Equation (3) summarizes the stiffness matrix of the base isolated structure:

$$\begin{bmatrix} T_1 \\ N_1 \\ \\ T_2 \\ N_2 \\ M_2 \end{bmatrix} = \begin{bmatrix} K_{SH} + 2\cdot\frac{12EI}{h^3} & 0 & -2\cdot\frac{12EI}{h^3} & 0 & -2\cdot\frac{6EI}{h^2} \\ 0 & K_{SV} + 2\cdot\frac{EA}{h} & 0 & -2\cdot\frac{EA}{h} & 0 \\ -2\cdot\frac{12EI}{h^3} & 0 & 2\cdot\frac{12EI}{h^3} & 0 & 2\cdot\frac{6EI}{h^2} \\ 0 & -2\cdot\frac{EA}{h} & 0 & 2\cdot\frac{EA}{h} & 0 \\ -2\cdot\frac{6EI}{h^2} & 0 & 2\cdot\frac{6EI}{h^2} & 0 & 2\cdot\left(\frac{4EI}{h}+\frac{EA}{h}\cdot\frac{L^2}{4}\right) \end{bmatrix} \begin{bmatrix} x_1 \\ y_1 \\ x_2 \\ y_2 \\ \theta_2 \end{bmatrix} \quad (3)$$

where K_{SH} and K_{SV} are respectively the total horizontal and vertical stiffness of the isolators. If a 2DOF system is assumed for the base isolated structures in the horizontal direction (x_1, x_2), the damping matrix is determined by the corresponding damping coefficients at the superstructure level c_2 and at the isolator level c_1. In particular c_2 is determined assuming that the superstructure is a SDOF system with a damping ratio ξ=0.05, while c_1 is determined assuming that the base isolated structure is a SDOF system with a damping ratio ξ=0.15.

The equations of motion are finally presented in the following:

$$\begin{bmatrix} m & 0 & 0 & 0 & 0 \\ 0 & m & 0 & 0 & 0 \\ 0 & 0 & m & 0 & 0 \\ 0 & 0 & 0 & m & 0 \\ 0 & 0 & 0 & 0 & \frac{mL^2}{12} \end{bmatrix} \begin{bmatrix} \ddot{x}_1 \\ \ddot{y}_1 \\ \ddot{x}_2 \\ \ddot{y}_2 \\ \ddot{\theta}_2 \end{bmatrix} + [K] \begin{bmatrix} x_1 \\ y_1 \\ x_2 \\ y_2 \\ \theta_2 \end{bmatrix} = - \begin{bmatrix} m & 0 & 0 & 0 & 0 \\ 0 & m & 0 & 0 & 0 \\ 0 & 0 & m & 0 & 0 \\ 0 & 0 & 0 & m & 0 \\ 0 & 0 & 0 & 0 & \frac{mL^2}{12} \end{bmatrix} \begin{bmatrix} \ddot{x}_g \\ \ddot{y}_g \\ \ddot{x}_g \\ \ddot{y}_g \\ 0 \end{bmatrix} \quad (4)$$

Thus, the vertical problem remains uncoupled from the others.

3) Structure isolated with the NSD

(

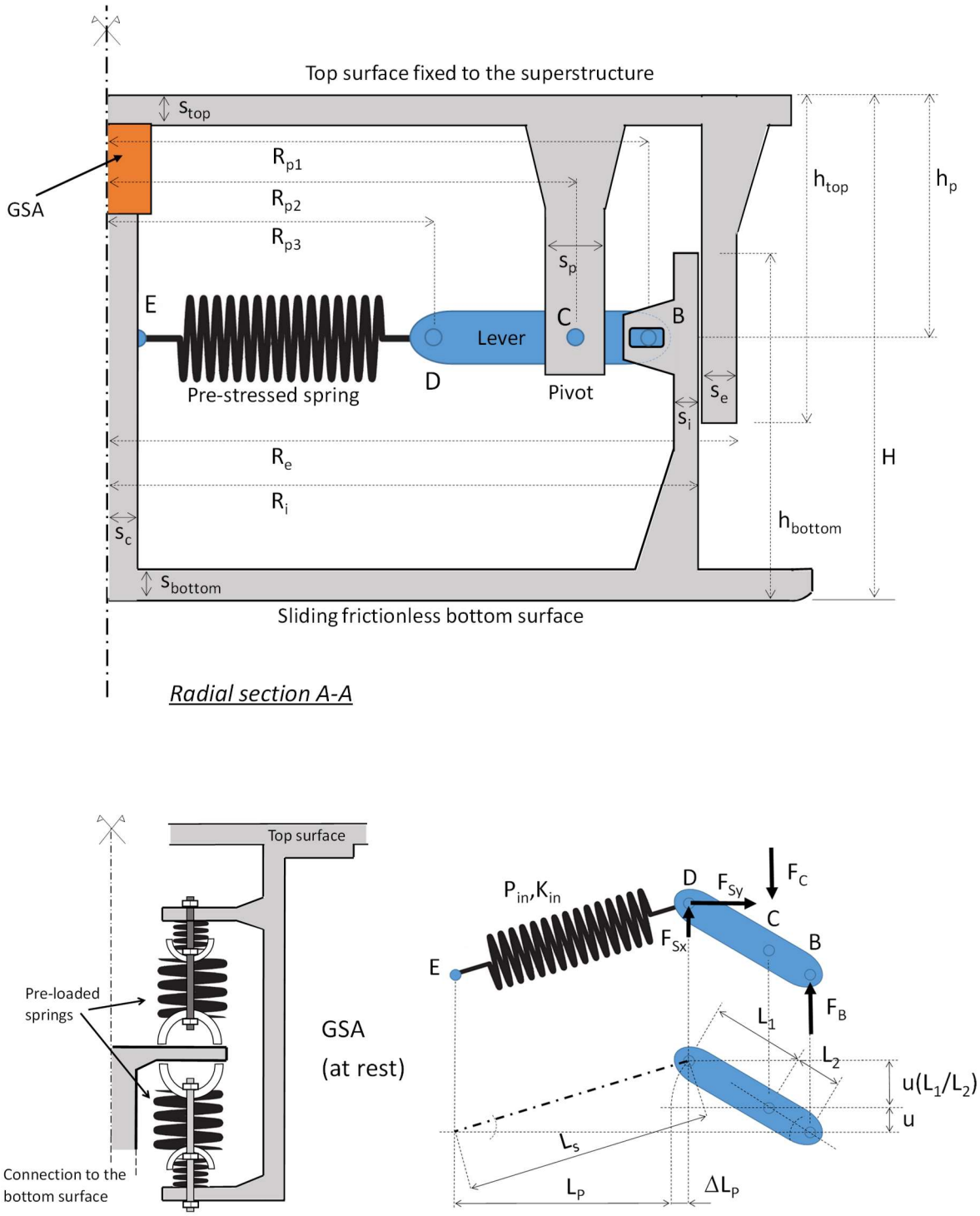

Figure 2*a)*:

The structure is the same as the isolated case, but the NSD is introduced at the base. The vertical isolation related to NSD is arranged to be uncoupled from the horizontal one (rubber bearings) and the NSD is linked to the structure at the base centroid of mass. Thus, it acts in the vertical direction only and provides no force in the horizontal direction. Hence, in the horizontal direction the rubber bearings ensure the base isolation, while the total vertical Force-Displacement law at the isolator level is the sum of both the NSD and the isolators contributions as they act in parallel. Practically the NSD is designed to get a specific Force-Displacement law as depicted by

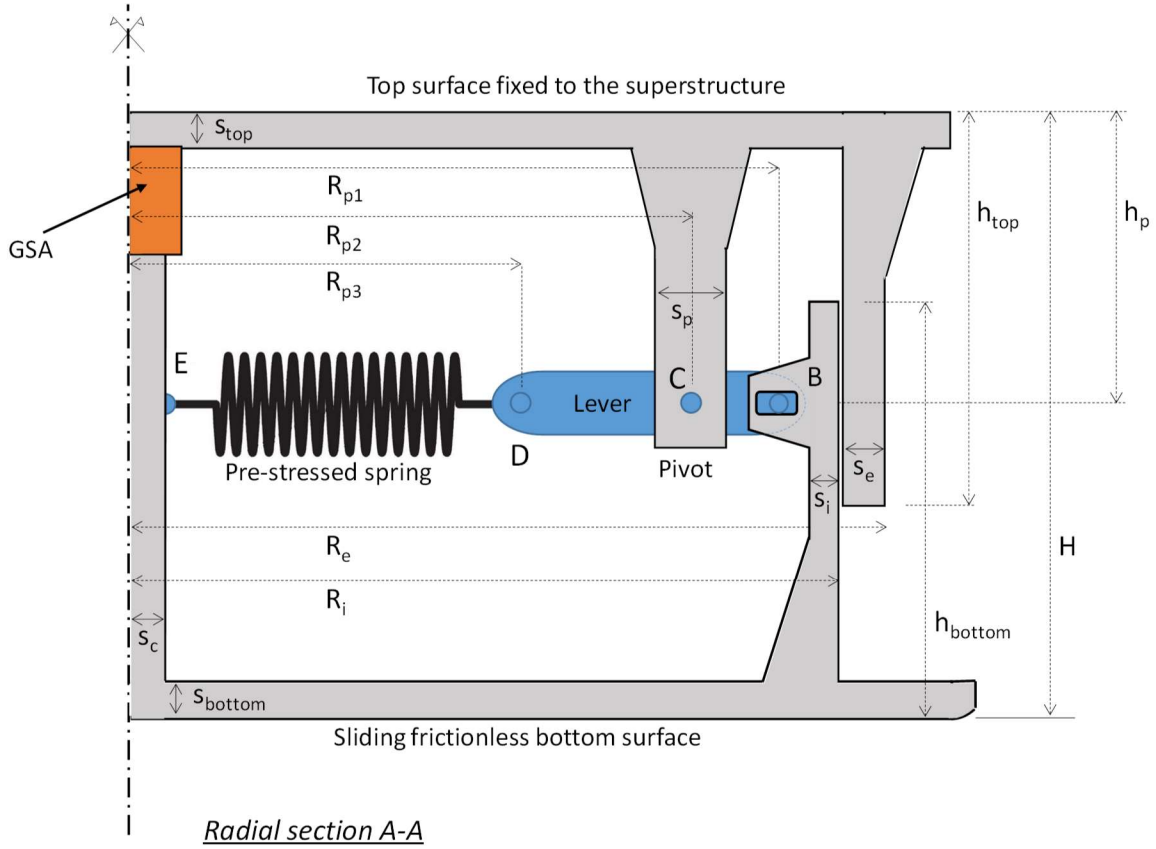

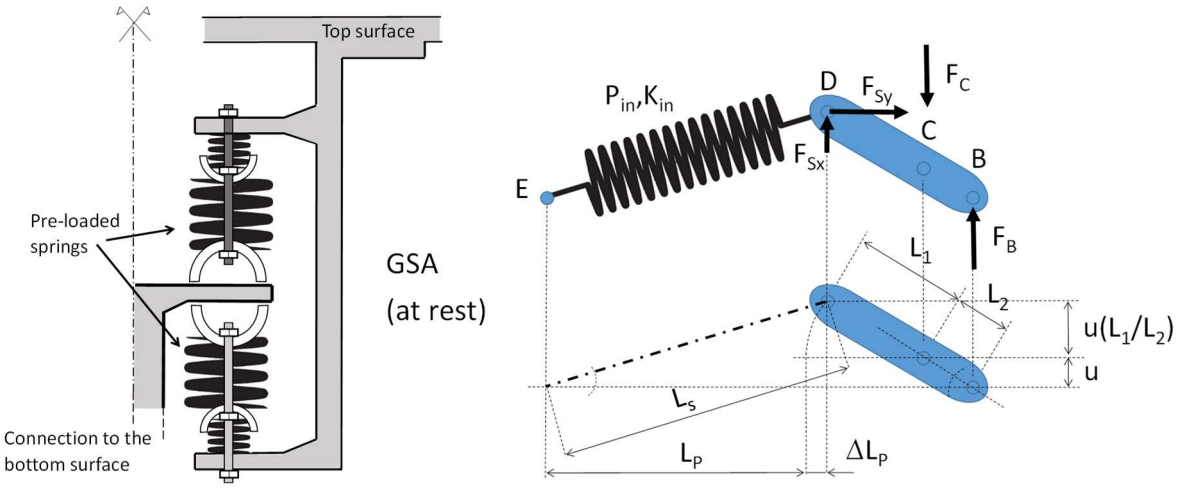

Figure 2b. It is nonlinear elastic and the parameters that characterize the behavior are the following:

- The stiffness of the first branch, equal to the total vertical isolators stiffness K_{NSD}.
- The stiffness of the second branch, equal to 10% of K_{NSD}.
- The gap-displacement δ when the NSD is engaged.

When the absolute value of the displacement is smaller than δ, the GSA provides a force opposite to the NSD, so that the structure behaves as if the NSD is not present. In this parametric study, five different gap-displacements are considered: 1-2-3-4-5 mm. The dynamic equations are the same as the isolated case, except for the second equation. The new one is detailed below:

$$m\ddot{y}_1 + \left(K_{SV} + 2\frac{EA}{h} \right) \cdot y_1 - 2\frac{EA}{h} \cdot y_2 + f_{NSD}(y_1) = -m\ddot{y}_g \tag{5}$$

As an extension of the previous structural configuration, the damping ratio of the superstructure is assumed *5%*, while it is assumed equal to *15%* for the rubber bearings, while NSD provides no damping.

Equations (4) and (5) of the NSD base isolated structural model outline how the vertical response results uncoupled from the others. Such quantitative aspect evidences the independent nature of

the 3-D isolation system, where the vertical isolation function is self-contained from the others components. Figure 2c summarizes the force-displacement characteristics in the vertical direction for the three structural configurations herein considered. All the numerical simulations have been performed using the software MATLAB [Matlab 2015].

Figure 2d depicts the 3D shape of the device that is also sketched in Figure 2a between the superstructure and the base foundation. It has a cylindrical shape, rigidly connected to the superstructure by the top surface and sliding frictionless to the base foundation through the bottom surface. Therefore, the uncoupled behavior between horizontal and vertical forces in the isolation system is provided. The material of the NSD components are assumed to be steel for the high stiffness and strength it provides.

The radial section A-A in Figure 2e describes the internal mechanism (at rest) that characterizes the typical radial module, as a slice. The main dimensions of the NSD components are also defined and have to be identified during the design process, considering the specific application of the NSD. The same radial modulus is replicated symmetrically in the NSD, e.g. for 4-6-8 times according to the NSD general dimensions. The NSD system employs highly pre-compressed helical springs in a double negative stiffness magnification mechanism that is produced through an internal lever that is fixed to the top NSD component by a pivot. Thus, the extension of the spring is magnified by the ratio of the lever. This solution reinterprets the one by Sarlis et al. [Sarlis et al., 2013] in a different framework.

It is worth noting that, as the blue lever tilts due to vertical displacements (Figure 2e), the R_{p1} distance (from the center to the far end of the lever) decreases due to R_{p2} is fixed. Therefore, to avoid locking in the mechanism, an horizontal slot on the rightmost pivot point of the lever is introduced.

Figure 2e reports also the position of the GSA mechanism within the NSD, while its detailed drawing (radial section at rest) is provided by Figure 2f. The GSA mechanism is characterized by the same working principles described in [Sarlis et al., 2013]. Therefore, the gap displacement δ, also termed the *NSD engagement displacement* (u_y'), is defined by eq. (17) in [Sarlis et al., 2013]. To define the analytical model of the negative stiffness mechanism, the deformed shape and the free body diagram have to be considered as in [Sarlis et al., 2013]. They are shown by Figure 2g without the GSA contribution, where P_{in} and K_{in} are respectively the precompression force and the stiffness of the spring. The vertical displacement u of the bottom surface of the device is equal to the displacements of points B and E (non-deformable members are assumed).

$$u = u_B = u_E = -u_D \frac{L_1}{L_2} \tag{6}$$

The spring length in the deformed configuration of the mechanism is computed as

$$L_S = \sqrt{(L_P + \Delta L_P)^2 + u^2(1 + \frac{L_1}{L_2})^2} \tag{7}$$

Where L_P is the length of the spring when u=0 (undeformed configuration) and the increment ΔL_P is due to the rotation of the lever around the pivot point C, as indicated in Figure 2g. This last one is defined as

$$\Delta L_P = L_1 - L_1\sqrt{1 - (\frac{u}{L_2})^2} \tag{8}$$

F_s is the force in the deformed configuration of the spring and its component can be derived as

$$F_S = P_{in} - k_{in}(L_s - L_P) \tag{9}$$

$$F_{Sx} = F_s \frac{u}{L_s}(1 + \frac{L_1}{L_2}) \tag{10}$$

$$F_{Sy} = F_s \frac{L_P + \Delta L_P}{L_s} \tag{11}$$

Writing the equilibrium of the lever around the pivot point C, the force exerted at point B can be computed as

$$F_B = \frac{u}{\sqrt{{L_2}^2 - u^2}} \left(\frac{F_S}{L_S} \left(1 + \frac{L_1}{L_2} \right) L_1 \sqrt{1 - \left(\frac{u}{L_2} \right)^2} + \frac{F_S (L_P + \Delta L_P)}{L_S} \frac{L_1}{L_2} \right) \quad (12)$$

GROUND MOTIONS

Civil engineering structures are subjected to 3-D seismic ground motions, however, even if both the horizontal and vertical components have been studied and considered in the design process, the vertical component of the ground motion has been sometimes underestimated [Ghaffarzadeh and Nazeri 2015; Nagarajaiah et al. 2013; Shakib and Fuladgar 2003]. Some building codes (e.g.[NEHRP 1994; UBC 1997]) also assume the vertical component of the ground motion to be a fraction of the horizontal component. However, in destructive earthquakes such as the 1989 Loma Prieta, 1994 Northridge, 1995 Kobe and 1999 Chi-Chi, it was found that vertical ground motion may equal or even exceed the local horizontal ground motion.

Several methods exist in literature for the ground motion selection to be used for time history analysis in the horizontal direction. A good summary of these existing methods can be found in [NIST 2011]. However, the focus is in the horizontal components, while there are not many criteria that can be used for the vertical components.

The principles herein adopted for the ground motion selection is to find earthquake records with high vertical component of ground motion, for example, by observing the PGA of the vertical component and by visual inspection of the displacement time history identifying the records with pulses. This condition is usually common in near field earthquakes where pulses are usually present both in the horizontal and vertical direction. The database adopted for the selection of

ground motions is the PEER database, while the selected set is shown in Table 1. The software OPENSIGNAL [Cimellaro 2013; Cimellaro and Marasco 2015; Marasco and Cimellaro 2017] has been used for the ground motion selection. Bi-dimensional analyses have been performed considering both the vertical and the maximum horizontal component. The mean response spectra of the selected set in term of displacements and accelerations in the vertical direction are shown in Figures 3 and 4 where the period of the analyzed structure in the vertical direction is also shown. As an example, a selected earthquake record is shown in Figure 5, where both the horizontal and the vertical components of ground motion in term of accelerations, velocities and displacements are given. As it can be observed, the vertical ground motion displacements are two times the horizontal displacements.

DESIGN OF THE ISOLATION SYSTEM AND DEVICES

Assessing the characteristics of the isolation system with the possible benefits coming from the NSD employment, the fixed base frame, the isolated scture and the isolated structure with NSD are considered. Focusing on the rubber bearings devices, assuming a starting range of horizontal stiffness for the isolators, the goal is to find the stiffness $\bar{K}_{SV}$ at which the NSD is more efficient in mitigating the vertical acceleration of the superstructure. To get a reasonable range, the first assumption is to consider a stiffness range that correspond to a horizontal period of vibration between 1 s and 4 s. Then, for identifying the total vertical stiffness of the isolators, the assumption is to have a ratio between the vertical and the horizontal reactions equal to 1000. The tests have been performed in the vertical direction using the earthquakes listed in Table 1. For each record, and for each stiffness, all the 5 values of gap-displacement δ are assumed.

The second part of the analysis concerns the design of the isolators. After the selection of the optimal vertical stiffness, the purpose is to design an isolation system that is able to withstand the displacements and the stresses induced by the seismic loading. The design must take in to account some requirements and verifications that appear in most codes: the control of the horizontal shear strain, the reduced area, the buckling and the stress in the materials.

Four geometrical and mechanical parameters characterize a rubber isolator. For each parameter, a range of possible values is selected and all the possible combinations are considered.

- the shear modulus of the elastomer G (0.4 – 0.8 – 1.4 MPa)
- the diameter D (from 0.3 m to 2.5 m)
- the number of rubber layers n (from 3 to 60)
- the thickness of each layer t (from 3 mm to 50 mm)

The formulas in Appendix A [AASHTO 2010] allow to identify the suitable solutions within the preliminary design ranges which have been considered in the numerical simulations. The next section is devoted to present results of the numerical simulations in terms of response mitigation by comparing the three different structural configurations herein considered. The last part of the study shows the comparison in terms of the amount of energy transmitted in the superstructure, as obtained by integration of the equations of motion.

NUMERICAL RESULTS

As described in the previous paragraph, first simulations are focusing on the research of the optimal vertical stiffness of the isolator at which the NSD is more effective in term of reduction of vertical acceleration component in the structure with respect to the isolated case. Obviously, the limitation of the displacements at the isolator level must be guaranteed.

It happens that the number of records that engages the NSD with the gap-displacement δ greater than 1 mm is negligible. However, with the value $\delta=1mm$ the results are satisfactory in terms of vertical acceleration mitigation. Therefore, for the aim of this preliminary study, all the analysis presented in the following are referred to this value.

Figure 6a shows the maximum vertical acceleration corresponding to each vertical stiffness for the earthquake Cape Mendocino. In Figure 6b the mean values and the standard deviations of all the ground motions considered are presented. With the same scheme, Figure 7 depicts the response of the maximum vertical displacement at the isolators' level, while in Figure 8 the minimum displacement is shown. They are measured from the absolute zero position of the isolators. It is important to separate the maximum and minimum displacement because of the different behavior of the rubber in tension and in compression. Tension is mainly due to NSD introduction but also to the ground motion in the vertical direction and the system dynamic: indeed, as highlighted by Figures 7 and 8, also the simple rubber bearings isolated structure experiences tension at certain stiffness ratio.

In Figure 7 and Figure 8, a dashed line represents the static vertical displacement that is a step function because it changes with the vertical stiffness.

Looking at the figures, a transition zone is observed where the stiffness is higher and the behavior of the two typologies of structures is very similar, because the displacements are smaller. Hence the NSD is engaged only few times. Instead, when the stiffness is small, a significant reduction of accelerations is obtained. Nevertheless, the highest tensile displacements are highlighted. The optimal stiffness is identified within the highlighted transition area, where the most satisfactory acceleration reduction in the vertical direction is reached, experiencing vertical relative displacements that are compatible with the isolated structure with rubber bearings.

A stiffness value of $\bar{K}_{SV}$=7.9x10^5 kN/m is adopted, representing the optimal value in terms of reduction of accelerations while limiting the displacements.

The next step consists in designing a reference isolator that is able to withstand the demand in terms of displacements and stresses, as from the preliminary analysis. After combining the independent parameters (*G*, *D*, *n*, *t*) described in previous paragraph (see also Figure A1 in Appendix A), the selected isolator has the characteristic in Table 2.

In this study, all the records used for the analyses generate large vertical displacements in the isolators. To withstand those displacements, it is necessary to improve the bearings deformability by managing the number and the thickness of the rubber layers, satisfying the design formulas in Appendix A. The characteristics of each isolator corresponding to each seismic record is reported in Table 3.

All the limitations have been satisfied except the (i) buckling condition in the Gazli quake and the (ii) the cavitation acceptable tensile limit that is exceeded under the Northridge record. About the first condition, the vertical load is smaller than the buckling load, but it is greater than its half (4.34 MPa). This means that the stiffness of the isolators is influenced and a nonlinear model in the analysis should be used. About the second issue, even if the theoretical cavitation limit is overcome for a small time period at the peak structural response, the design of the isolation system for a real application should be re-evaluated. However, these questions are not within the aim of this work that represents a preliminary stage of the design, so the unsatisfactory responses related to these quakes have been disregarded.

It is worth mentioning, about tensile forces in base isolation systems, the studies by Roussis (e.g. [Roussis 2009]) on special connections between the devices and the structure. Such solutions that remove the possibility of the vertical load on the isolator becoming tensile are also allowed by the

standard [STANDARDIZATION 2009]. However, the implementation of any uplift prevention mechanism would modify the behavior of the isolation system and should then be included in the model of analysis.

The comparison of the response of the three adopted typologies of structures is shown in Figure 9 and Figure 10. The figures highlight how NSD is very efficient in reducing the vertical acceleration. For some earthquakes the reduction is relevant, while for others is less. However the case with the NSD is almost always the best option.

Figures 9 and 10 also show that the displacements for the two isolated cases (isolated structure and structure isolated with negative stiffness) are comparable in tension and in the compression, with the only exception of Northridge earthquake.

Figure 11 shows that the results in terms of vertical drifts in the superstructure are satisfactory. There are cases in which the reduction is significant, while in other cases there is no significant reduction. Furthermore, Figure 12 shows the forces needed in the negative stiffness devices necessary to achieve such performances that are normalized with respect to the total weight of the building. The capacity of the NSD to limit the seismic energy transmitted to the structure during the earthquake is also investigated. Figure 13 shows the comparison of the considered structural typologies. The records of Cape Mendocino and Northridge are shown and, in both cases, when the NSD is employed, the amount of input energy in the structure is reduced with respect to fixed base and simple isolated versions.

SUMMARY AND CONCLUSIONS

The paper deals with the insertion of negative stiffness devices in parallel with rubber bearings in a base isolated building to control the vertical response. The structure is isolated horizontally with

a system of elastomeric bearings and vertically with the NSD in parallel with the isolators. Both the horizontal and the vertical stiffness elements are implemented independently and a 3-D base isolation with uncoupled reaction components is achieved.

A standard SDOF steel portal frame have been considered in the analysis to test the effectiveness of the proposed configuration with respect to traditional fixed base and isolated ones. A set of earthquake records typical of the near-fault regions with the characteristic of pulse shape has been selected to perform the nonlinear dynamic analyses.

The numerical analyses show that by implementing negative stiffness devices in the vertical direction, the vertical accelerations are smaller than in a structure simply isolated. However, consistently with the base isolation theory, there are increments of displacements at the isolator level. Thus, the NSD, if properly designed, is able to reduce the vertical seismic forces with respect to the traditional base isolated systems, without considerably increasing the absolute and relative displacements. The NSD is also able to reduce the input energy transferred to the superstructure with respect to the base-isolated structure.

The limitations of the present study and the adopted assumptions can be summarized as follows. (i) The results in terms of internal forces in the negative stiffness devices show maximum intensities that are 2-3 times larger than the structural weight. It indicates a design concept that is complex to be implemented in practical applications and likely restricted to special conditions (light highly sensitive equipment or sculptures and artistic masterworks). This aspect is also emphasized considering the very small required gap (about 1 mm) in the negative stiffness system. (ii) A 2D simplified model of the devices with linear elastic and viscous characteristics is adopted at this stage to analyze the effectiveness of the different parameters in the performance of the 3-D base isolation system. Next steps will consider the development of a prototype and consequently

a more refined representation of the 3D isolation system. (iii) Analyses highlight satisfactory results, even if device buckling condition and cavitation acceptable tensile limit in rubber material have been exceeded in single cases. However, these issues overcome the aim of this work and could be solved in the further step of the study with a more definite representation of the design.

ACKNOWLEDGMENTS

The research leading to these results has received funding from the European Research Council under the Grant Agreement n° ERC_IDEAL RESCUE_637842 of the project IDEAL RESCUE-Integrated Design and Control of Sustainable Communities during Emergencies.

REFERENCES

AA Sarlis, D. P., MC Constantinou, AM Reinhorn, S Nagarajaiah, D Taylor "Negative stiffness device for seismic protection of structures - an analytical and experimental study." *Proc., 3rd ECCOMAS Thematic Conference on Computational Methods in Structural Dynamics and Earthquake Engineering - COMPDYN 2011*.

AASHTO [2010]. "Guide specifications for seismic isolation design, 3rd Edition." A. A. o. S. H. a. T. Officials-AASHTO, ed.Washington, DC.

Abe, M., Yoshida, J., and Fujino, Y. [2004]. "Multiaxial behaviors of laminated rubber bearings and their modeling. I: Experimental study." J Struct Eng-Asce, 130(8), 1119-1132.

Asai, T., Yoshida, N., Masui, T. and Araki, Y. [2008]. "Vertical Seismic Isolation Device Using Constant Load Supporting Mechanisms." Journal of Structural and Construction Engineering AIJ(73), 8.

Attary, N., Symans, M., Nagarajaiah, S., Reinhorn, A. M., Constantinou, M. C., Sarlis, A. A., Pasala, D. T. R., and Taylor, D. [2015]. "Performance Evaluation of Negative Stiffness Devices for Seismic Response Control of Bridge Structures via Experimental Shake Table Tests." Journal of Earthquake Engineering, 19(2), 249-276.

Cimellaro, G. P. [2013]. "Correlation in spectral accelerations for earthquakes in Europe." Earthquake Engineering & Structural Dynamics, 42(4), 623-633.

Cimellaro, G. P., Lavan, O., and Reinhorn, A. M. [2009]. "Design of Passive systems for controlled inelastic structures." Earthquake Engineering & Structural Dynamics, 38(6), 783-804.

Cimellaro, G. P., and Marasco, S. [2015]. "A computer-based environment for processing and selection of seismic ground motion records: OPENSIGNAL." Frontiers in Built Environment, 1:17.

Ghaffarzadeh, H., and Nazeri, A. [2015]. "The effect of the vertical excitation on horizontal response of structures." Earthq Struct, 9(3), 625-637.

H Iemura, O. K., A Toyooka, I Shimoda "Development of the friction-based passive negative stiffness damper and its verification tests using shaking table." *Proc., The 14th World Conference on Earthquake Engineering (14WCEE)*.

Harvey, P. S. [2016]. "Vertical Accelerations in Rolling Isolation Systems: Experiments and Simulations." J Eng Mech, 142(3).

Hoque, M. E., Mizuno, T., Ishino, Y. and Takasaki, M. [2011]. "A three-axis vibration isolation system using modified zero-power controller with parallel mechanism technique." Mechatronics, 21(6), 8.

ID Aiken, J. K., FF Tajirian [1989]. "Mechanics of Low Shape Factor Elastomeric Seismic Isolation Bearings." University of California, Berkeley, CA.

Iemura, H., Igarashi, A., Pradono, M. H., and Kalantari, A. [2006]. "Negative stiffness friction damping for seismically isolated structures." Structural Control & Health Monitoring, 13(2-3), 775-791.

Iemura, H., and Pradono, M. H. [2003]. "Application of pseudo negative stiffness control to the benchmark cable-stayed bridges." Journal of structural control, 10(3-4), 187-203.

Inoue, K., Fushimi, M., Moro, S., Morishita, M., Kitamura, S. and Fujita, T. [2004]. "Development of Three-Dimensional Seismic Isolation System for Next Generation Nuclear Power Plant." *13th World Conference on Earthquake Engineering*Vancouver, B.C., Canada.

JM Kelly, E. Q. [1990]. "Testing and Evaluation of CEGB Isolation System." University of California, Berkeley, CA.

Kelly, J. M. [1988]. "Base Isolation in Japan." University of California, Berkeley, CA.

Kelly, J. M., and Van Engelen, N. C. [2016]. "Fiber-Reinforced Elastomeric Bearings for Vibration Isolation." J Vib Acoust, 138(1).

Kitayama, S., Constantinou, M.C. and Lee, D. [2016]. "". [2016]. "Procedures and Results of Assessment of Seismic Performance of Seismically Isolated Electrical Transformers with Due Consideration for Vertical Isolation and Vertical Ground Motion Effects." *MCEER-16-0010 Report*, 180.

Lee, C. M., Goverdovskiy, V., and Temnikov, A. [2007]. "Design of springs with 'negative' stiffness to improve vehicle driver vibration isolation." Journal of Sound and Vibration, 302(4-5), 865-874.

Li, X. Y., Xue, S. D., and Cai, Y. C. [2013]. "Three-dimensional seismic isolation bearing and its application in long span hangars." Earthq Eng Eng Vib, 12(1), 55-65.

Marasco, S., and Cimellaro, G. P. [2017]. "A new energetic-based ground motion selection and modification method limiting the dynamic response dispersion and preserving the median demand." Bulletin of Earthquake Engineering, DOI: 10.1007/s10518-017-0232-5, 1-21.

Matlab. 2015. The MathWorks, Inc. The Language of Technical Computing

Mochida, Y., Kida, N. and Ilanko, S. [2015]. "Base Isolator of Vertical Seismic Vibration Using a Negative Stiffness Mechanism." Vibration Engineering and Technology of Machinery, 7.

Molyneaux, W. [1957]. "Supports for vibration isolation."

Molyneaux, W. G. [1957]. "Supports for vibration isolation." A.R.C. - C.P. No.322, Aeronautical Research Council.

Morishita, M., Inoue, K. and Fujita, T. [2004]. "Development Of Three-Dimensional Seismic Isolation Systems For Fast Reactor Application." Journal of Japan Association for Earthquake Engineering, 4(3), 6.

Nagarajaiah, S., Pasala, D. T. R., Reinhorn, A., Constantinou, M., Sirilis, A. A., and Taylor, D. [2013]. "Adaptive Negative Stiffness: A New Structural Modification Approach for Seismic Protection." Adv Mater Res-Switz, 639-640, 54-66.

Nagarajaiah, S., Reinhorn, A. M., Constantinou, M. C., D., T., Pasala, D. T. R., and Sarlis, A. A. "True adaptive negative stiffness: A new structural modification approach for seismic protection." *Proc., Proc. 5th World Conf. on Structural Control and Monitoring*.

NEHRP [1994]. "Recommended provisions for seismic regulations for new buildings." *FEMA 222A*.

NIST [2011]. "Selecting and Scaling Earthquake Ground Motions for Performing Response-History Analyses." *NIST GCR 11-917-15*, N. I. o. S. a. T. N. u. t. N. E. H. R. P. (NEHRP), ed.

Okamura, S., Kamishima, Y., Negishi, K., Sakamoto, Y., Kitamura, S., and Kotake, S. [2011]. "Seismic Isolation Design for JSFR." J Nucl Sci Technol, 48(4), 688-692.

P. Alabuzhev, A. G., L. Kim, G. Migirenko, V. Chon, P. Stepanov [1989]. Vibration Protecting and Measuring Systems with Quasi-Zero Stiffness, Hemisphere Publishing Corporation, New York

Pasala, D. T. R., Sarlis, A. A., Nagarajaiah, S., Reinhorn, A. M., Constantinou, M. C., and Taylor, D. [2013]. "Adaptive Negative Stiffness: New Structural Modification Approach for Seismic Protection." J Struct Eng, 139(7), 1112-1123.

Pasala, D. T. R., Sarlis, A. A., Reinhorn, A. M., Nagarajaiah, S., Constantinou, M. C., and Taylor, D. [2014]. "Simulated Bilinear-Elastic Behavior in a SDOF Elastic Structure Using Negative Stiffness Device: Experimental and Analytical Study." Journal of Structural Engineering, 140(2).

Pasala, D. T. R., Sarlis, A. A., Reinhorn, A. M., Nagarajaiah, S., Constantinou, M. C., and Taylor, D. [2015]. "Apparent Weakening in SDOF Yielding Structures Using a Negative Stiffness Device: Experimental and Analytical Study." J Struct Eng, 141(4).

Perotti, F., Domaneschi, M., and De Grandis, S. [2013]. "The numerical computation of seismic fragility of base-isolated Nuclear Power Plants buildings." Nucl Eng Des, 262, 189-200.

Platus, D. [1991]. "Negative-stiffness-mechanism vibration isolation system." Proceedings of the SPIE, vibration control in microelectronics, optics, and metrology, 1619, 11.

Platus, D. L. a. F., D.K. [2007]. "Negative-stiffness vibration isolation improves reliability of nanoinstrumentation." Laser Focus World, 43(10), 3.

Reinhorn, A. M., Lavan, O., and Cimellaro, G. P. [2009]. "Design of controlled elastic and inelastic structures." Earthq Eng Eng Vib, accepted for publication October 13, 2009.

Roussis, P. C. [2009]. "Panayiotis C. Roussis." Journal of Structural Engineering ASCE, 135(12), 10.

S Nagarajaiah, A. R., MC Constantinou, DTR Pasala, AA Sarlis " True adaptive negative stiffness: A new structural modification approach for seismic protection." *Proc., 5th World Conf. on Structural Control and Monitoring*.

Sarlis, A. A., Pasala, D. T. R., Constantinou, M. C., Reinhorn, A. M., Nagarajaiah, S., and Taylor, D. P. [2013]. "Negative Stiffness Device for Seismic Protection of Structures." J Struct Eng, 139(7), 1124-1133.

Sarlis, A. A., Pasala, D. T. R., Constantinou, M. C., Reinhorn, A. M., Nagarajaiah, S., and Taylor, D. P. [2016]. "Negative Stiffness Device for Seismic Protection of Structures: Shake Table Testing of a Seismically Isolated Structure." J Struct Eng, 142(5).

Shakib, H., and Fuladgar, A. [2003]. "Effect of vertical component of earthquake on the response of pure-friction base-isolated asymmetric buildings." Eng Struct, 25(14), 1841-1850.

Soong, T. T., and Cimellaro, G. P. [2009]. "Future directions on structural control." journal of Structural control and Health Monitoring 16(1), 7-16.

STANDARDIZATION, E. C. F. [2009]. "EUROPEAN STANDARD - EN 15129 - Anti-seismic devices." *Isolators*.

Suhara, J. "Research on 3D base isolation system applied to new power reactor 3D seismic isolation device with rolling seal type air spring: part 1 - Paper #K09e4, ." *Proc., SMiRT 17*.

UBC [1997]. "The Uniform Building Code."

Viti, S., Cimellaro, G. P., and Reinhorn, A. M. [2006]. "Retrofit of a hospital through strength reduction and enhanced damping " Smart Structures and Systems, An international Journal, 2(4), 339-355.

APPENDIX A

The demand parameter is introduced as function of the isolator diameter D and the vertical displacement u_v. It has the following expression (Figure A1):

$$\alpha = \frac{u_V \cdot D}{A_r} \tag{6}$$

The reduced area A_r has the expression below so it is a function of the diameter and the horizontal displacement u_h.

$$A_r = \frac{D^2}{2} \cdot \left[\arccos\left(\frac{u_H}{D} \right) - \frac{u_H}{D} \cdot \sin\left(\arccos\left(\frac{u_H}{D} \right) \right) \right] \tag{7}$$

The first step consists in the calculation of the max parameter α during the earthquake. Several simulations has been performed with different records and different diameters of the isolators corresponding to a range of horizontal stiffness that lead to periods of vibration between 2s and 4s. The analysis in the horizontal and vertical direction have been decoupled to reduce the computational efforts. The next step is the exclusion of the isolators that do not respect the conditions below:

1) Excessive deviation of the effective stiffness K_{SV} from $\overline{K}_{SV}$

$$K_{SV} = \frac{E' \cdot A}{n \cdot t} \tag{8}$$

where E' is the compression modulus of the rubber, n the number of rubber layers, t the thickness of each rubber layer. The limit was fixed to 5%.

2) Horizontal stiffness K_{SH} that gives an horizontal period $T < 2$s or $T > 4$s.

The last condition prevents large displacements while the first represents a region in which the isolation is not effective.

$$K_{SV} = \frac{G \cdot A}{n \cdot t} \tag{9}$$

where G is the shear modulus of the rubber, A the area of the isolator.

3) Excessive shear strain

$$\gamma_H = \frac{u_H}{n \cdot t} < 2 \tag{10}$$

4) Horizontal displacement greater than the diameter D (null reduced area is zero and no vertical load can be carried on).

$$u_H < D \tag{11}$$

5) Isolators susceptible of buckling. In a rubber isolator under large displacement, when the vertical load exceeds the critical load P_{crit}, the isolator loses stability.

$$P_{crit} = P_{crit0} \cdot \frac{A_r}{A} \tag{12}$$

that is

$$\alpha < \frac{0,5}{K_{SV}} \cdot \frac{\sqrt{2} \cdot \pi \cdot G \cdot D^3}{16 \cdot n \cdot t^2} \tag{13}$$

Where P_{crit0} is the buckling load under vertical load only.

Actually when the vertical load approaches the buckling load, the stiffness is strongly modified. The model is assumed linear, so the ratio between the actual load and the critical one must be smaller than 0.5. Within this limit, the horizontal stiffness undergoes little influence.

6) Rubber compression. The vertical load distributed in the reduced area produce a stress that must be limited to an acceptable fixed threshold (σ_R).

$$\frac{K_{SV} \cdot u_V}{A_r} < \sigma_R \tag{14}$$

That is

$$\frac{K_{SV} \cdot \alpha}{D} < \sigma_R \tag{15}$$

7) Total strain of the rubber. The combination of vertical and horizontal deformations must be limited:

$$\gamma_{tot} = \gamma_H + \gamma_V = \frac{u_H}{n \cdot t} + \frac{3 \cdot D}{2 \cdot E'} \cdot \frac{K_{SV} \cdot u_V}{A_r} < 5 \tag{16}$$

8) Max stress in the steel plates (t_s). This condition is used for the design of the thickness.

$$t_S > 1,3 \cdot \frac{K_{SV} \cdot u_V}{A_r} \cdot \frac{2 \cdot t}{f_{yk}} > 2mm \tag{17}$$

The inner plates must be greater than 2 mm. The outer (t_{S0}) are assumed 20 mm. Then the total height of the isolator is evaluated as:

$$h_{IS} = n \cdot t + (n-1) \cdot t_S + 2 \cdot t_{S0} \tag{18}$$

NGA #	Earthquake Name	Date	M_W	Depth [km]	Station	Accel.	Type	Epicentral Distance [km]	Site Vs30 [m/s]
825	Cape Mendocino	1992	7	9.6	Cape Mendocino	000 Z	Near fault - Pulse	10.36	514
1176	Kocaeli, Turkey	1999	7.4	15	Yarimca	060 Z	Near fault - Pulse	19.3	297
77	San Fernando	1971	6.6	13	Pacoima Dam	164 Z	Near fault - Pulse	11.86	2016
1605	Duzce, Turkey	1999	7.1	10	Duzce	270 Z	Near fault - Nonpulse	1.61	276
1231	Chi-Chi, Taiwan	1999	7.6	6.8	CHY080	N Z	Near fault - Nonpulse	31.65	553
230	Mammoth Lakes-01	1980	6.3	9	Convict Creek	180 Z	Near fault - Nonpulse	1.43	338
879	Landers	1992	7.3	7	Lucerne	260 Z	Near fault - Pulse	44.02	685
126	Gazli, USSR	1976	6.8	18.2	Karakyr	090 Z	Near fault - Nonpulse	12.82	660
1063	Northridge-01	1994	6.7	17.5	Rinaldi Rec.Sta	228 Z	Near fault - Pulse	10.91	282
143	Tabas, Iran	1978	7.4	5.8	Tabas	LN Z	Near fault - Nonpulse	55.24	767

Table 1 – List of the 10 earthquake records adopted in the analyses

G	0,4	Mpa	Shear modulus
D	1500	mm	Diameter
n	12	-	Number of rubber layers
t	49	mm	Thickness of each rubber layer
$n \cdot t$	588	mm	Total thickness of the rubber
t_s	2	mm	Thickness of each steel plate
t_0	20	mm	Thickness of the outer steel plate
h	650	mm	Isolator total height
S	7,65	-	Shape factor
A	1,77	m^2	Area of the isolator
K_{SH}	2404,3	N/mm	Design total horizontal stiffness
K_{SV}	789419,7	N/mm	Design total vertical stiffness
ΔK_{SV}	0,02	%	Deviation from the target stiffness
K_{SV} / K_{SH}	328	-	Stiffness ratio
T_H	2,3	s	1st vibration horizontal period
T_V	0,13	s	1st vibration vertical period

Table 2 – Properties of the rubber isolators

Earthquake	Rubber shear strain		Rubber total strain		Steel tension		Rubber compression		Rubber tension
	γ_H	$\gamma_{H\ MAX}$	γ_{tot}	$\gamma_{tot\ MAX}$	σ_{S-}	f_{yk}	σ_{R-}	σ_{Rmax}	σ_{R+}
	[-]	[-]	[-]	[-]	[MPa]	[MPa]	[MPa]	[MPa]	[MPa]
Cape Mendocino	0.39	<2	1.00	<5	124	<450	1.9	<4,34	0.4
Kocaeli	0.44		0.91		89		1.4		-
Duzce	0.56		1.01		93		1.5		-
Mammoth Lakes	0.18		0.62		82		1.3		-
Landers	0.62		1.13		110		1.7		0.1
Gazli	0.45		1.82		322		5.1		1.3
Northridge	0.74		1.80		256		4.0		1.8
Tabas	0.75		1.37		151		2.4		1.3

Table 3 – Design verification of the Isolator

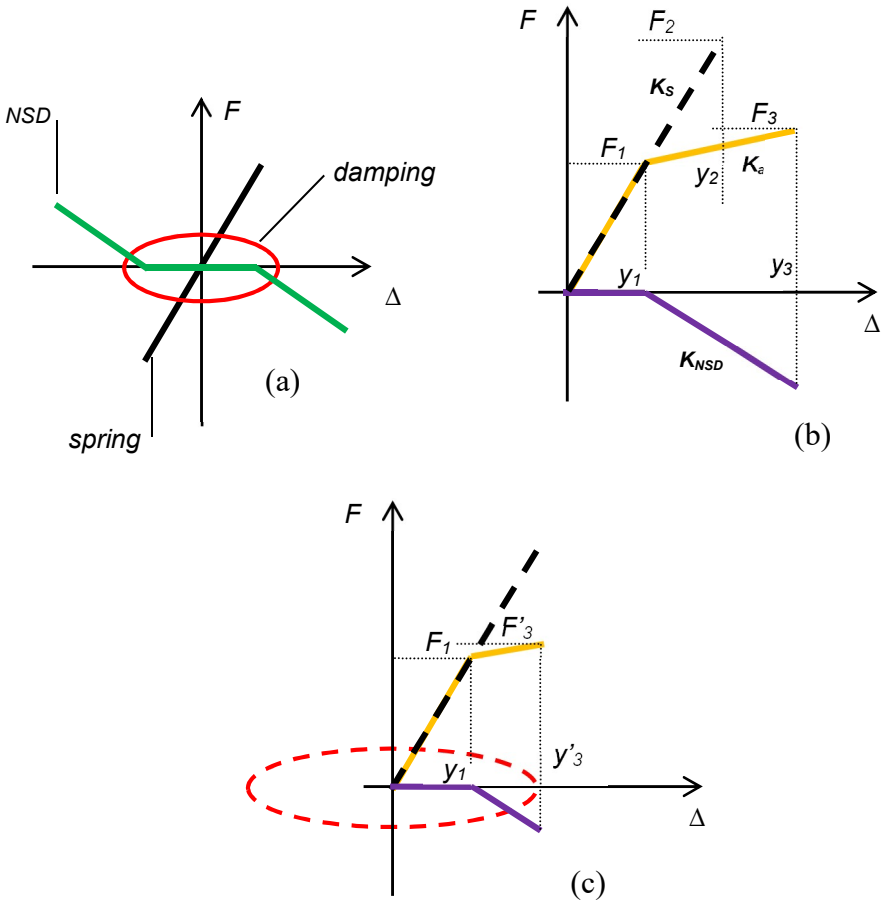

Figure 1: Schematic Force-Displacement behavior of the NSD implemented in the structure. (a) Force components, (b) structure + NSD, (c) effect of damper in parallel with the structure + NSD

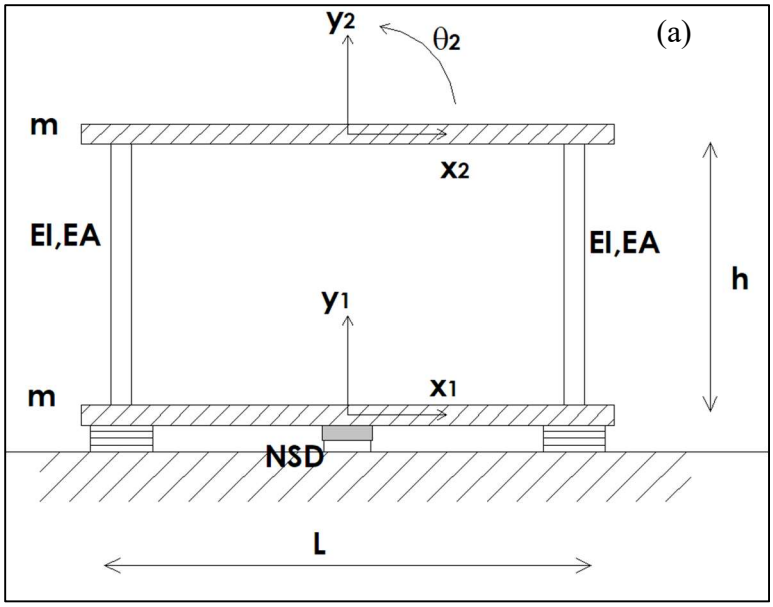
y2
θ2
(a)
m
x2
EI,EA
EI,EA
h
y1
m
x1
NSD
L

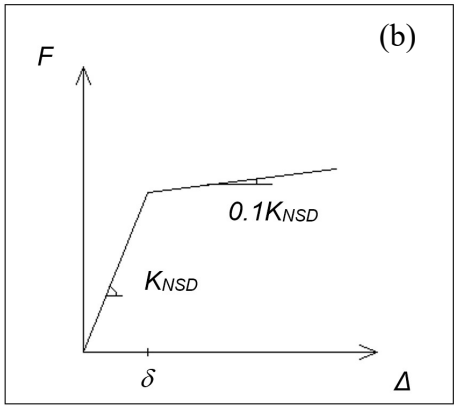
(b)
F
0.1K_NSD
K_NSD
δ
Δ

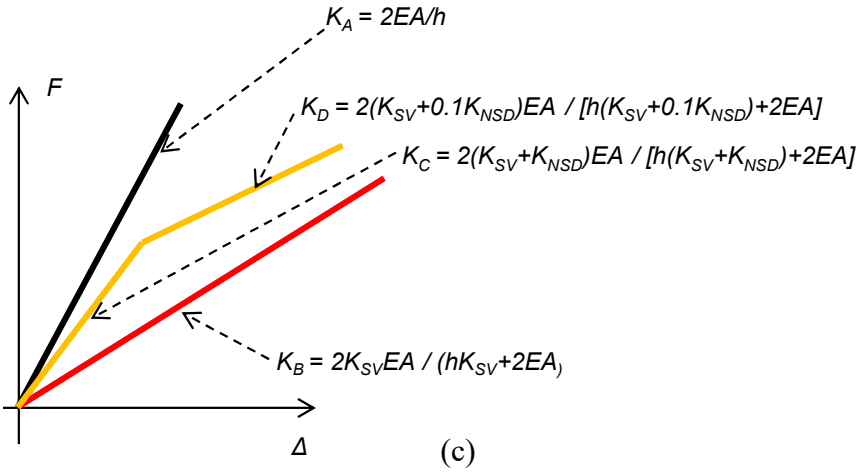
K_A = 2EA/h
F
K_D = 2(K_SV+0.1K_NSD)EA / [h(K_SV+0.1K_NSD)+2EA]
K_C = 2(K_SV+K_NSD)EA / [h(K_SV+K_NSD)+2EA]
K_B = 2K_SVEA / (hK_SV+2EA)
Δ

(c)

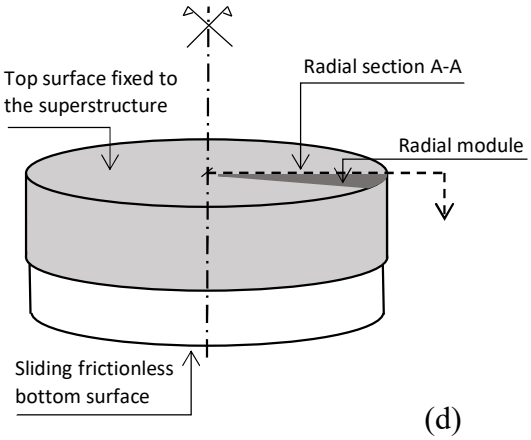
Top surface fixed to the superstructure
Radial section A-A
Radial module
Sliding frictionless bottom surface

(d)

3D view

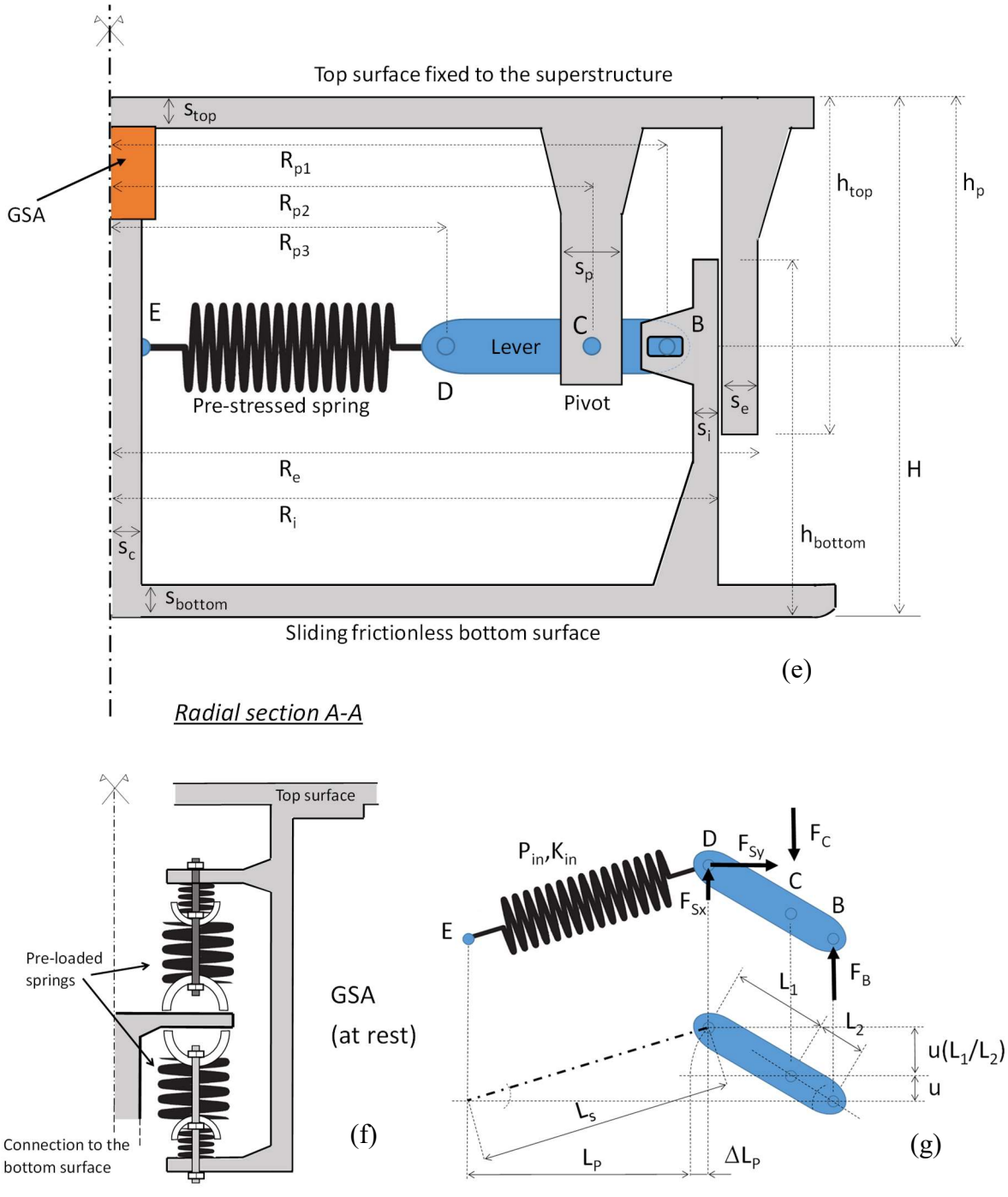

Figure 2: (a) scheme of the structure isolated with NSD. (b) Total vertical $F\Delta$ law at the NSD isolator level. (c) vertical stiffness: K_A for fixed base structure, K_B with columns and rubber bearing stiffness in series. If NSD are added in parallel with rubber bearings K_C is the total pre-yielding stiffness and K_D the post-yielding one. The 3D scheme of the NSD device (d) with the detail of the characteristic radial module (e). Detail of the GSA radial section (f). Deformed shape and the free body diagram of the NSD mechanism (g).

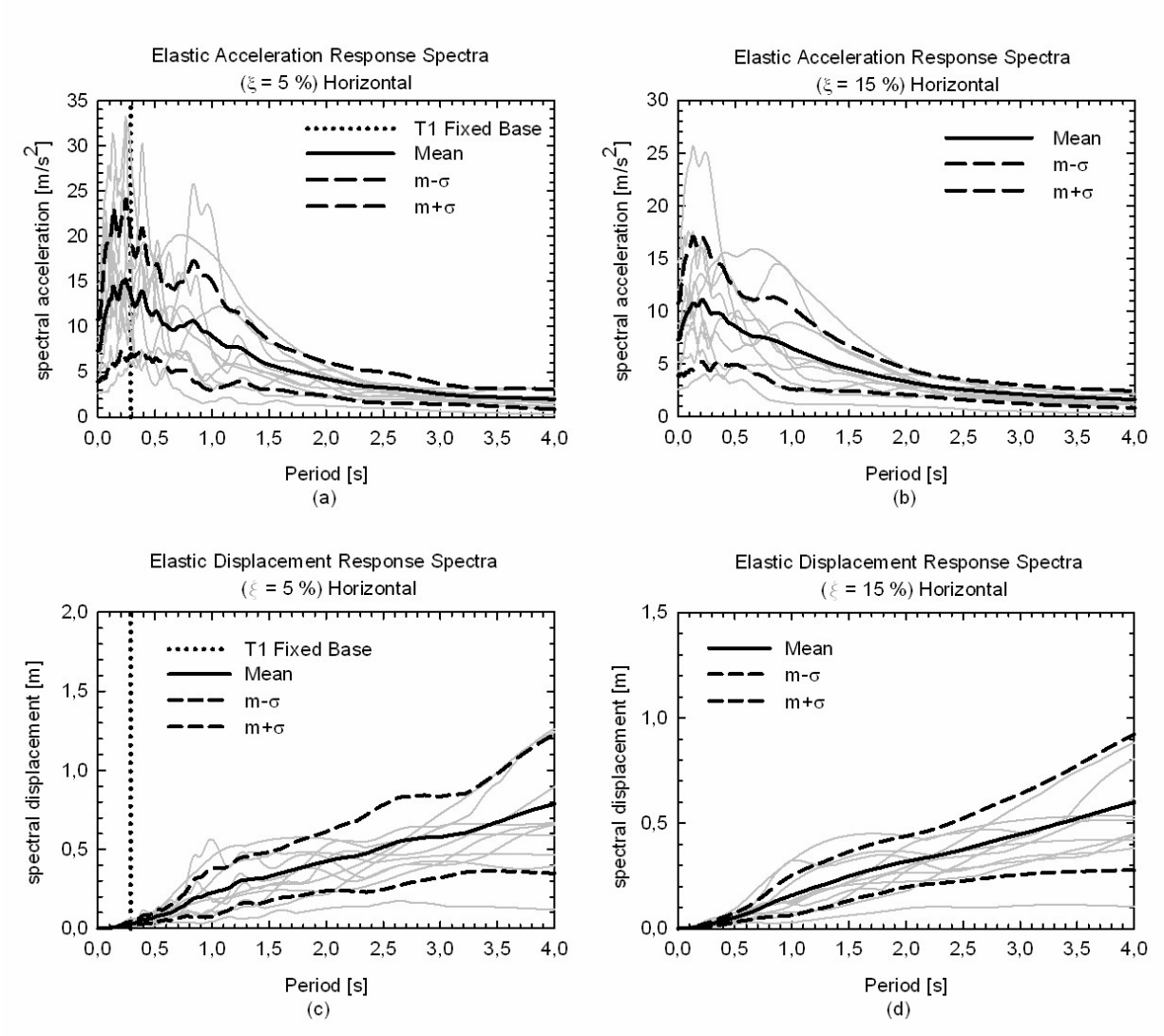

Figure 3 : Horizontal acceleration response spectrum for (a) ξ=5%; (b) ξ=15%; Displacement response spectrum for (c) ξ=5%; (d) ξ=15%.

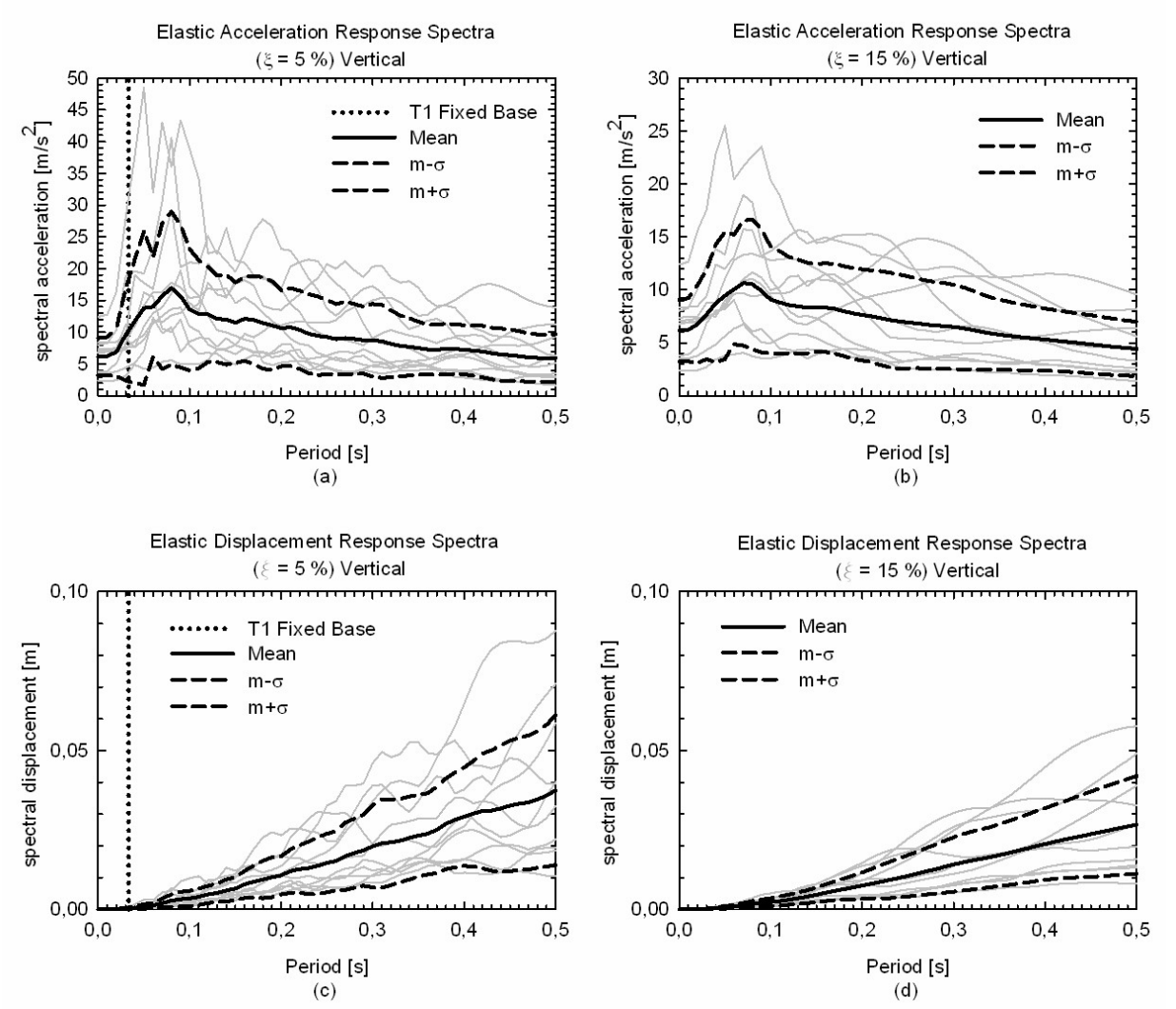

Figure 4 : Vertical acceleration response spectrum for (a) ξ=5%; (b) ξ=15%; Displacement response spectrum for (c) ξ=5%; (d) ξ=15%.

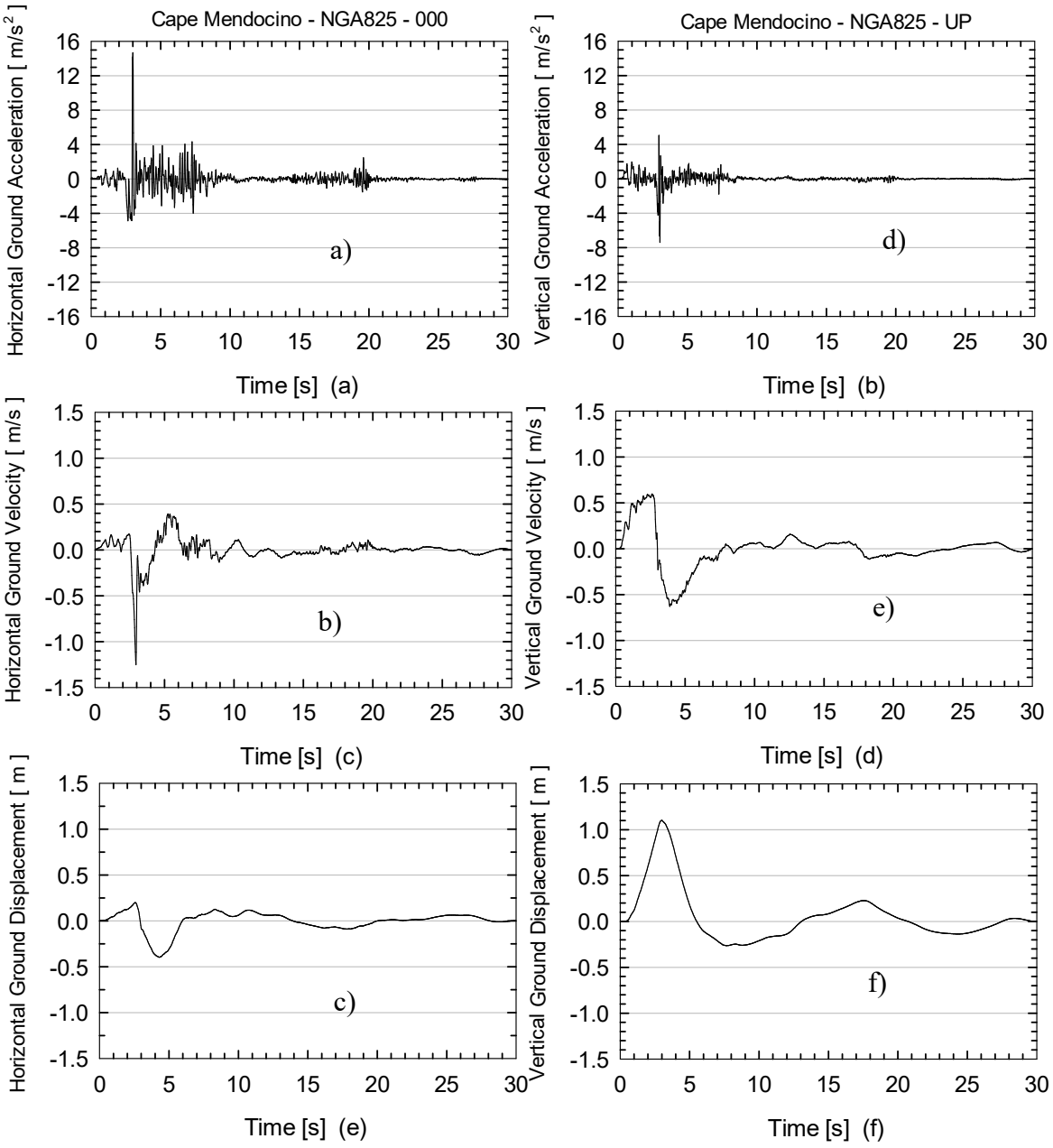

Figure 5: Horizontal time history of Cape Mendocino earthquake: (a) acceleration; (b) velocity; (c) displacements. Vertical time history of Cape Mendocino earthquake: (d) acceleration; (e) velocity; (f) displacements

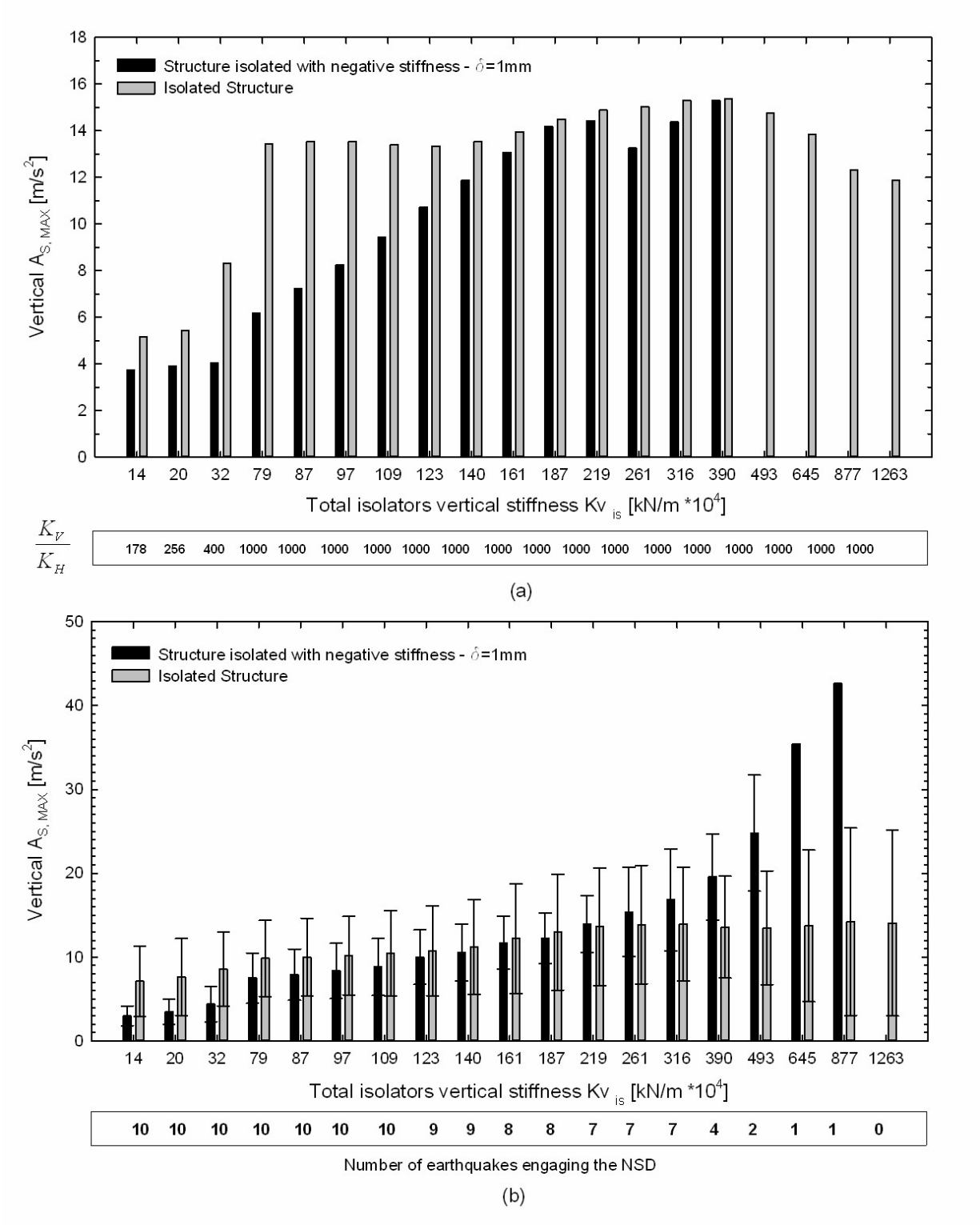

Figure 6 Comparison of vertical accelerations for traditional base isolation vs. NSD for different vertical stiffnesses. Cape Mendocino (a), mean values of all earthquake records (b)

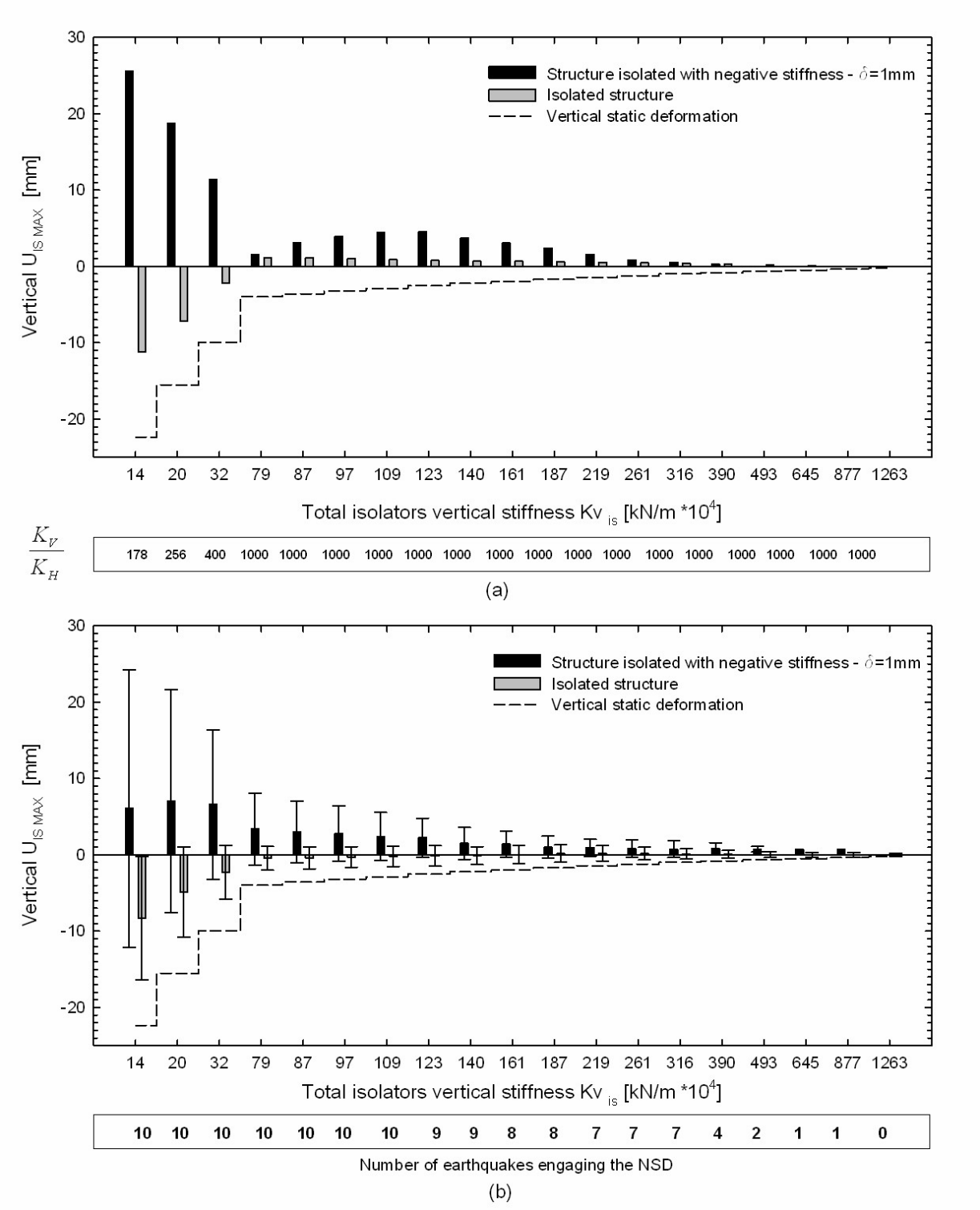

Figure 7 Comparison of maximum vertical displacement at the isolator level for traditional base isolation vs. NSD for different vertical stiffnesses. Cape Mendocino (a), mean values of all earthquake records (b). Maximum uplift: 24 mm in the structure with NSD.

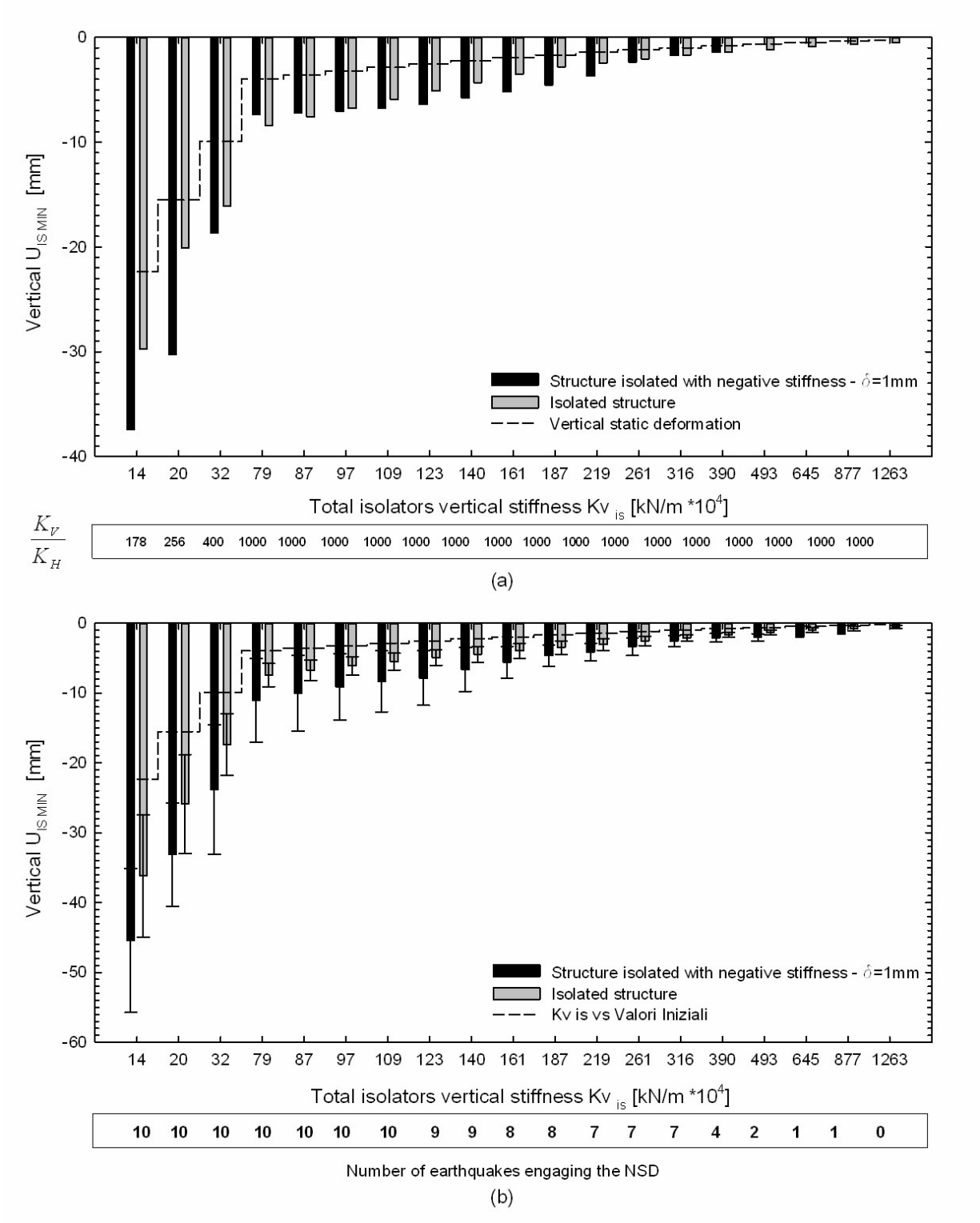

Figure 8 Comparison of minimum vertical displacement at the isolator level for traditional base isolation vs. NSD for different vertical stiffnesses. Cape Mendocino (a), mean values of all earthquake records (b). Minimum displacement: 56 mm in the structure with NSD.

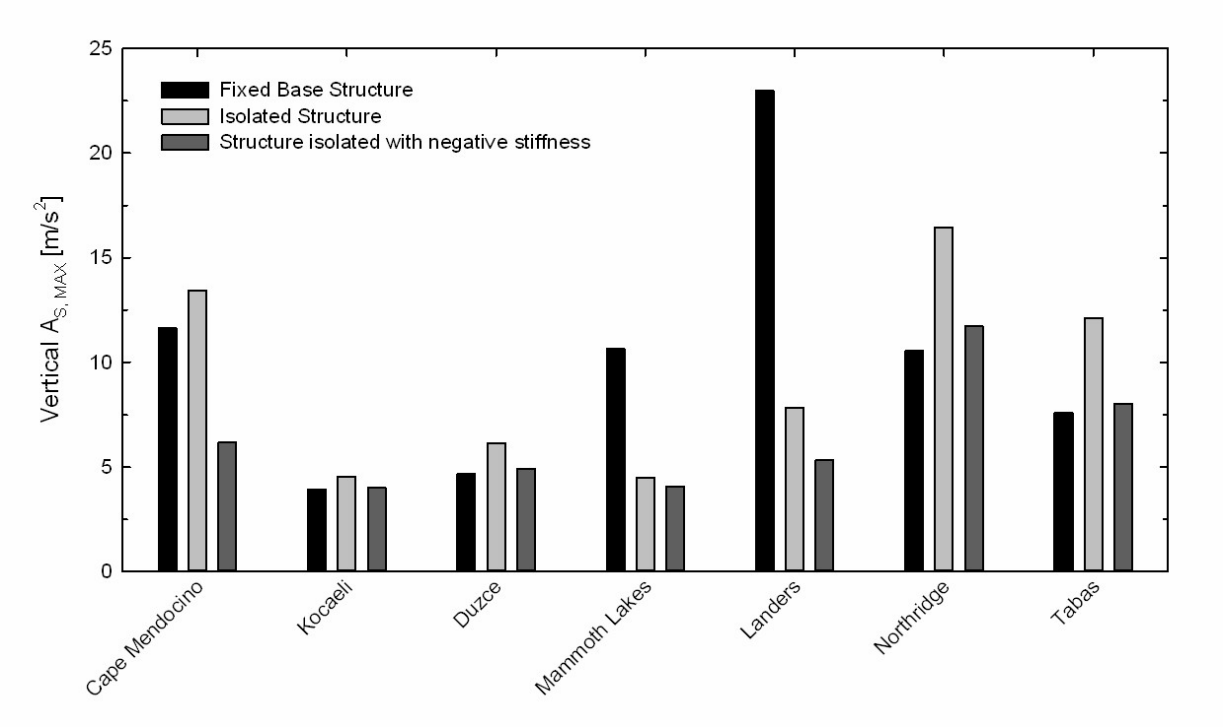

Figure 9 Comparison of vertical accelerations of the proposed design retrofit strategy vs. the traditional base isolated structure for different earthquake events;

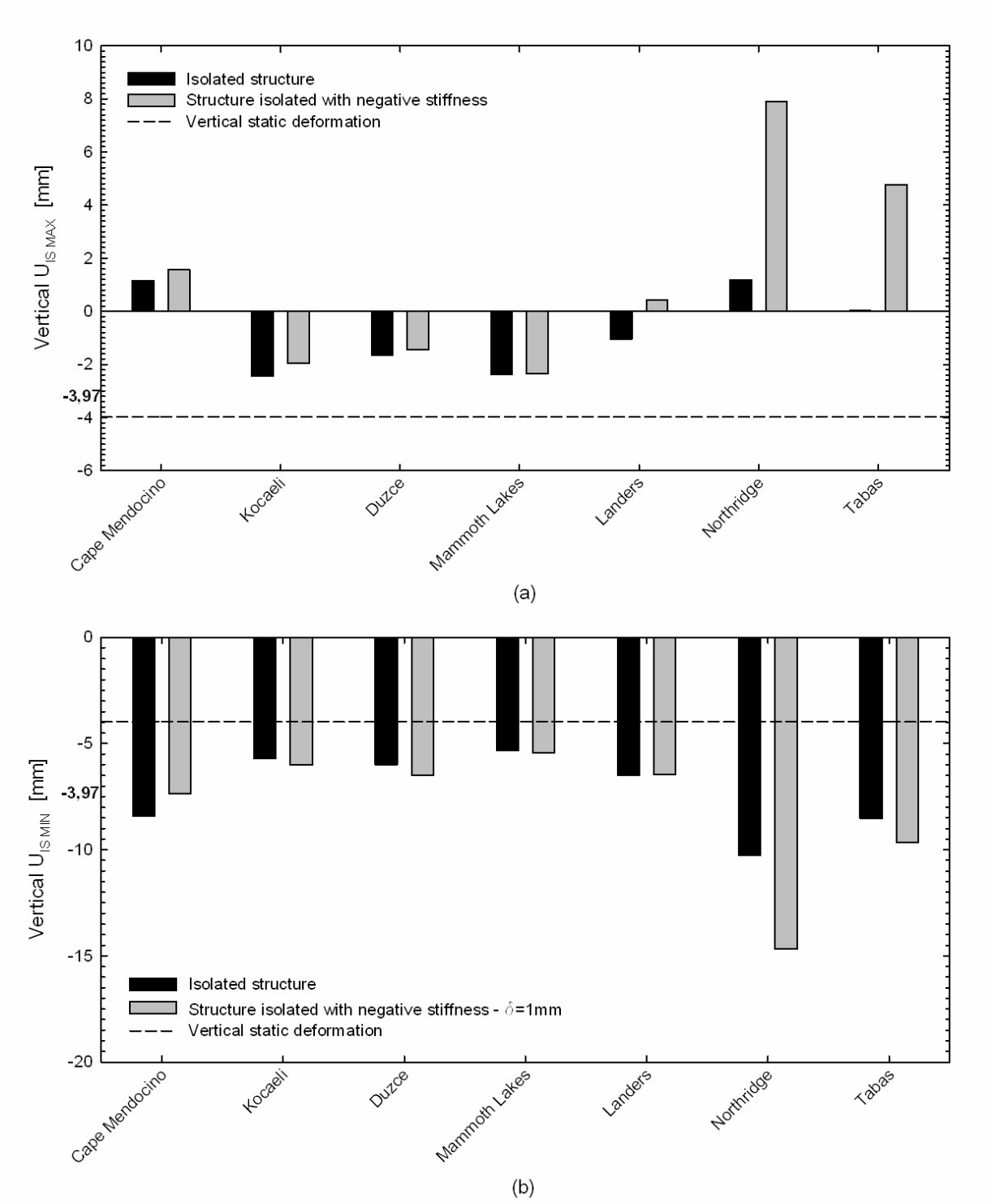

Figure 10 Comparison of vertical isolator displacement of the proposed design retrofit strategy vs. the traditional base isolated structure for different earthquake events. Max isolator vertical displacement (a), min isolator vertical displacement (b)

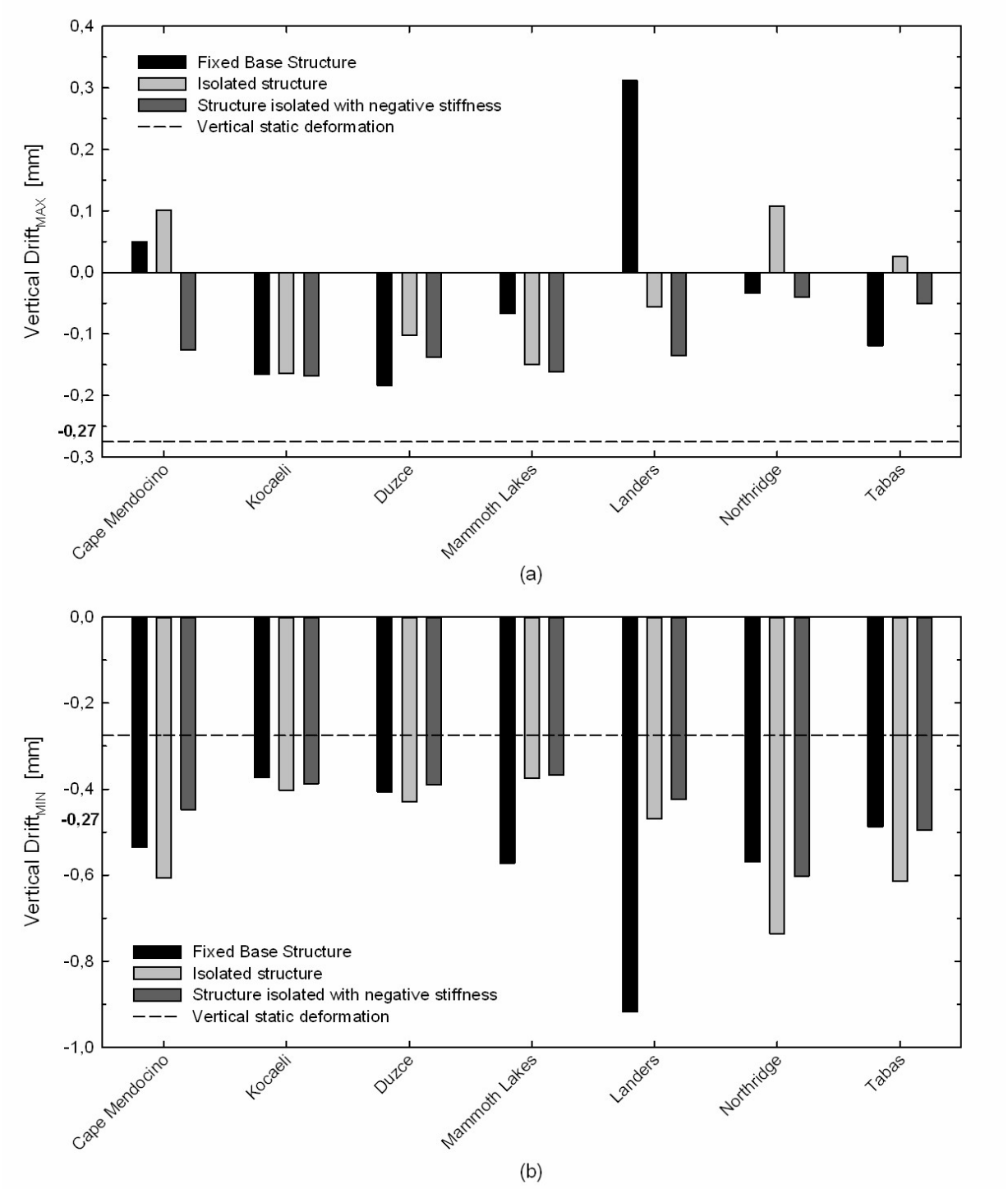

Figure 11 Comparison of vertical drift of the proposed design retrofit strategy vs. the traditional base isolated structure for different earthquake events. Max vertical drift (a), min vertical drift (b)

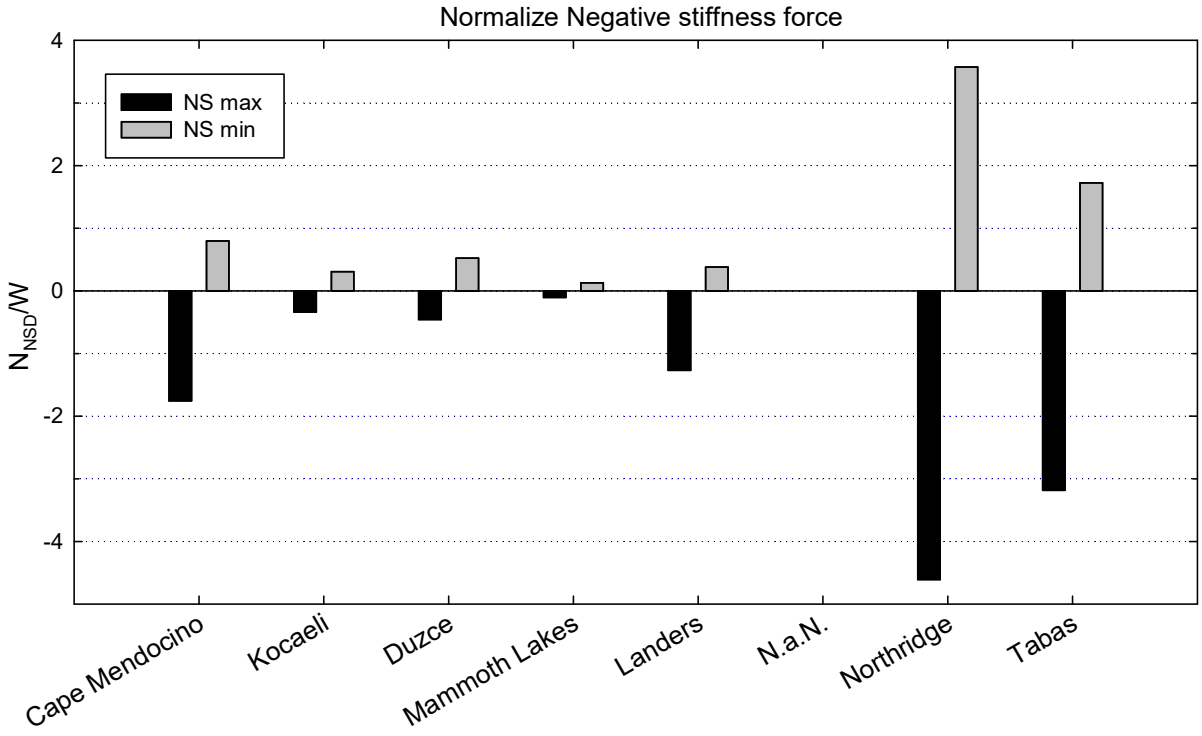

Figure 12 Total negative stiffness force needed and normalized with respect to the weight of the building

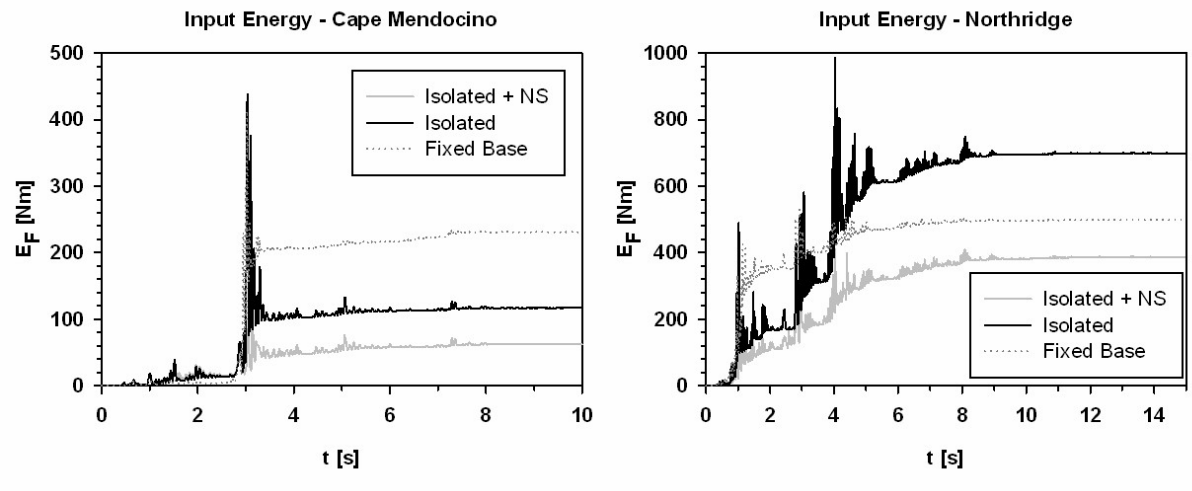

Figure 13 Vertical input energy for different earthquake events and retrofit strategies

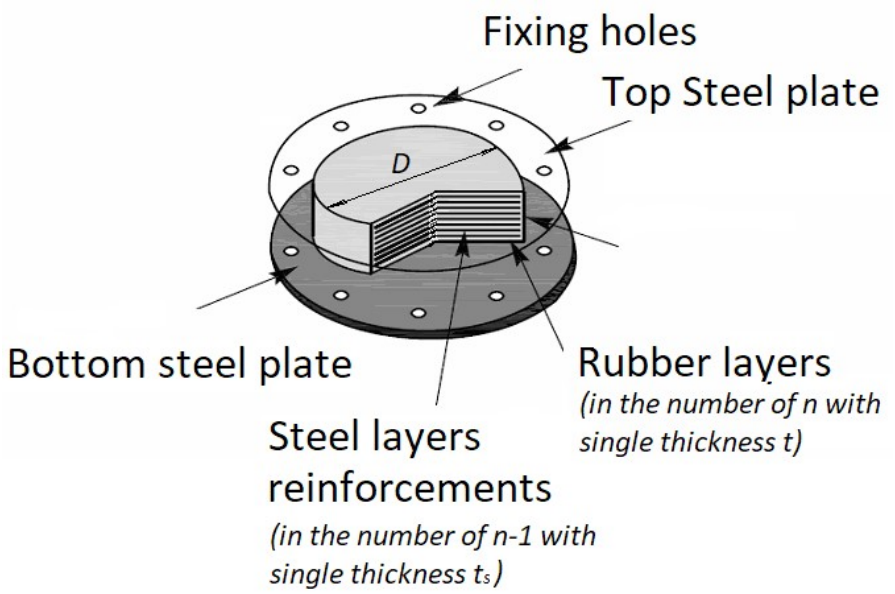

Figure A1 Rubber bearings with main characteristics